AMERICAN SOCIETY FOR MICROBIOLOGY | Molecular and Cellular Biology

Differential Involvement of the Npl4 Zinc Finger Domains of SHARPIN and HOIL-1L in Linear Ubiquitin Chain Assembly Complex-Mediated Cell Death Protection

Satoshi Shimizu,[a,b] Hiroaki Fujita,[a] Yoshiteru Sasaki,[a] Tatsuaki Tsuruyama,[c] Kazuhiko Fukuda,[b] Kazuhiro Iwai[a]

Department of Molecular and Cellular Physiology, Graduate School of Medicine, Kyoto University, Kyoto, Japan[a]; Department of Anesthesia, Kyoto University Hospital, Kyoto, Japan[b]; Department of Diagnostic Pathology, Kyoto University Hospital, Kyoto, Japan[c]

The linear ubiquitin chain assembly complex (LUBAC) participates in NF-κB activation and cell death protection. Loss of any of the three LUBAC subunits (catalytic HOIP, accessory HOIL-1L, or accessory SHARPIN subunit) leads to distinct phenotypes in mice and human. cpdm mice (chronic proliferative dermatitis in mice [cpdm]) that lack SHARPIN exhibit chronic inflammatory phenotypes, whereas HOIL-1L knockout mice exhibit no overt phenotypes, despite sharing highly homologous ubiquitin-like (UBL) and Npl4 zinc finger (NZF) domains. Here, we intercrossed mice lacking HOIL-1L and SHARPIN and found that reduction of HOIL-1L in cpdm mice exacerbated inflammatory phenotypes without affecting characteristic features of cpdm disease, whereas reduction of SHARPIN in HOIL-1L knockout mice provoked no overt phenotypes. Hence, loss of SHARPIN and reduction of LUBAC triggers cpdm phenotypes. We found that the NZF domain of SHARPIN, but not that of HOIL-1L, is critical for effective protection from programmed cell death by enhancing the recruitment of LUBAC to the activated TNFR complex. The binding activity to K63-linked ubiquitin chains that the NZF domain of SHARPIN, but not that of HOIL-1L, possesses appears to be involved in the recruitment. Thus, selective recognition of ubiquitin chains by NZFs in LUBAC underlies the regulation of LUBAC function.

The ubiquitin system plays crucial roles in regulating a vast array of physiological processes by, in most cases, conjugating various types of ubiquitin chains onto target proteins (1–5) since different ubiquitin chains are decoded by distinct ubiquitin-binding proteins in a chain type-specific manner to modulate their functions or fates (6, 7). Ubiquitin chains are thought to be largely generated through covalent linkage between a C-terminal glycine residue of one ubiquitin to one of the seven lysine residues within another ubiquitin. Recently, we discovered a novel ubiquitin E3 ligase complex termed the linear ubiquitin chain assembly complex (LUBAC), which specifically conjugates a C-terminal glycine residue of one ubiquitin to an N-terminal methionine residue of another ubiquitin to generate the linear ubiquitin chain (8). LUBAC participates in canonical NF-κB activation by conjugating linear ubiquitin chains onto the NF-κB essential modulator (NEMO) (9, 10). This appears to be a critical step in the activation of the IKK complex, the principal regulator of the NF-κB cascade (9–12). In addition, LUBAC exhibits a novel function to antagonize programmed cell death provoked by various stimuli, including tumor necrosis factor receptor (TNFR) signaling, although the precise molecular mechanisms remain unknown (13–18).

LUBAC is composed of three subunits: a catalytic subunit, HOIP, and two accessory subunits, SHARPIN and HOIL-1L. The last two subunits share ubiquitin-like (UBL) and Npl4 zinc finger (NZF) domains with high amino acid sequence similarity (8, 13–15, 19, 20). HOIP also carries two NZF domains, NZF1 and NZF2 (8). Since the NZF domains serve as the ubiquitin-binding modules, LUBAC seems to possess multiple ubiquitin-binding activities (19, 21). Previous reports show that loss of any of the three LUBAC subunits results in distinct phenotypes in mice and humans, indicating the differential roles of each subunit in LUBAC functions. For example, loss of the catalytic subunit, HOIP, causes embryonic lethality in mice with aberrant programmed cell death, including vascular endothelial cells at embryonic day 10.5 (E10.5) (16).

Intriguingly, mice lacking SHARPIN or HOIL-1L display different phenotypes unique to each deletion, despite the structural similarity of the two accessory subunits. For example, SHARPIN-null cpdm mice (chronic proliferative dermatitis in mice [cpdm]) exhibit severe inflammatory phenotypes characteristic of chronic proliferative dermatitis (22–24) and multiorgan pathology with immunological disorders (25–27), presumably due to augmented programmed cell death in response to TNFR signaling (17, 18, 28). In contrast, our HOIL-1L knockout (KO) mice fail to exhibit any overt inflammatory disorders (9). The mechanism underlying the phenotypical difference between cpdm and HOIL-1L KO mice is of great interest, since residual LUBAC content and NF-κB activation upon stimulation with cytokines such as TNF-α are both profoundly diminished in either case (13).

In the present study, we intercrossed mice lacking either SHARPIN or HOIL-1L and subjected the offspring to a number of experimental analyses to disclose the coordinate and distinct functions of the two accessory subunits. Mice carrying mutations in both SHARPIN and HOIL-1L exhibited midgestational lethality at E10.5, similar to mice lacking the ubiquitin ligase activity of

Received 3 December 2015 **Returned for modification** 31 December 2015
Accepted 5 March 2016

Accepted manuscript posted online 14 March 2016

Citation Shimizu S, Fujita H, Sasaki Y, Tsuruyama T, Fukuda K, Iwai K. 2016. Differential involvement of the Npl4 zinc finger domains of SHARPIN and HOIL-1L in linear ubiquitin chain assembly complex-mediated cell death protection. Mol Cell Biol 36:1569–1583. doi:10.1128/MCB.01049-15.

Address correspondence to Kazuhiro Iwai, kiwai@mcp.med.kyoto-u.ac.jp.

HOIP (HOIP$^{\Delta linear/\Delta linear}$ mice), or HOIP-null mice (16). While introduction of one cpdm (SHARPIN-null) allele into HOIL-1L KO (HOIL-1L$^{-/-}$ SHARPIN$^{+/cpdm}$) mice had no obvious effect, HOIL-1L reduction in SHARPIN$^{cpdm/cpdm}$ (HOIL-1L$^{+/-}$ SHARPIN$^{cpdm/cpdm}$) mice significantly exacerbated the severity of cpdm diseases at early onset. These results suggest that SHARPIN is essential for the inhibition of inflammatory diseases, while HOIL-1L affects disease severity only when SHARPIN is absent; our data further suggest that loss of both accessory subunits abolishes LUBAC ligase activity. Additionally, we dissected the molecular mechanisms underlying SHARPIN involvement in protection against cell death and found that the ubiquitin recognition activity of the SHARPIN NZF domain, but not that of the HOIL-1L NZF domain, contributed to cell death protection by effectively recruiting LUBAC to the activated TNFR complex upon stimulation with tumor necrosis factor alpha (TNF-α). Taken together, these findings clarify the differential involvement of the LUBAC accessory subunits and their NZF domains in regulating LUBAC function.

MATERIALS AND METHODS

Mice, preparation of cells, and cell culture. HOIL-1L$^{-/-}$ mice and HOIP$^{\Delta linear/\Delta linear}$ mice were generated as described previously (9, 29). SHARPIN$^{cpdm/cpdm}$ mice were obtained from the Jackson Laboratory. All mice were maintained under specific-pathogen-free conditions in the animal facilities of Kyoto University. All animal protocols were approved by Kyoto University. For timed mating of mice, a single male was mated with one or two females. The day that a vaginal plug was detected was considered embryonic day 0.5 (E0.5). Primary mouse embryonic fibroblasts (MEFs) were harvested from the various mice, immortalized with simian virus 40 (SV40) large T antigen, and cultured as described previously (9).

TUNEL assay. E10.5 embryos were fixed in 10% buffered formalin, followed by paraffin embedding. Serial sections (4-μm thick) were prepared and used for TUNEL (terminal deoxynucleotidyltransferase-mediated dUTP-biotin nick end labeling) staining according to the manufacturer's instructions (*in situ* cell death detection kit, fluorescein; Roche Life Science). Quantification was performed by counting the number of TUNEL-positive and -negative cells by using a BZ-900 fluorescence microscope (Keyence). At least three independent fields per section were scored from each embryo ($n = 3$).

Histology. Samples were fixed in 10% buffered formalin, followed by paraffin embedding. Sections were then prepared and stained with hematoxylin and eosin (H&E) and/or with periodic acid-Schiff stain (PAS reagent) according to standard protocols.

Immunohistochemistry. Paraffin-embedded sections from mice were dewaxed with xylene three times for 5 min and rehydrated through gradient ethanol series of 100%, 90%, and 80% for 10 min and then washed with distilled water. For antigen retrieval, sections were heated in citrate buffer (pH 6.0) for 10 min at 95°C in a microwave oven and then cooled to room temperature. MEFs were cultured in collagen-coated chamber slide glass (Matsunami Glass Ind., Ltd.). After the indicated treatments, samples were fixed with freshly prepared 4% paraformaldehyde in phosphate-buffered saline (PBS) for 10 min at room temperature. Samples were then washed with PBS three times. For immunohistochemical analyses of the phosphorylated form of mixed-lineage kinase domain-like (pMLKL), the samples were permeabilized by methanol for 10 min at −20°C, washed with PBS three times, and blocked by 5% bovine serum albumin (BSA) in PBS at room temperature for 1 h. The samples for immunohistochemical analyses for cleaved caspase 3 were washed with PBS and blocked by 1% BSA–5% goat serum–0.3% Triton X-100 containing PBS at room temperature for 1 h. The samples were then incubated with the appropriate primary antibody diluted in the blocking buffer at a 1:100 dilution at 4°C overnight. Samples were washed with PBS three times and then incubated with the appropriate Alexa Fluor 546-conjugated secondary antibody at a 1:1,000 dilution for 1 h at room temperature. After the samples were washed with PBS three times, they were mounted with a coverslip using ProLong gold antifade reagent with DAPI (4′,6-diamidino-2-phenylindole) (ThermoFisher Scientific), followed by subsequent analyses using a BZ-900 fluorescence microscope (Keyence) or confocal laser scanning fluorescence microscopes (Olympus model FV1000D).

RT-PCR. For quantitative real-time PCR (RT-PCR), total RNA from the dorsal skin of mice of the indicated genotypes was isolated by using the RNeasy minikit (Qiagen) according to the manufacturer's instructions. The RNA was reverse transcribed into cDNA by using a high-capacity RNA-to-cDNA kit (Applied Biosystems). Each experiment was normalized to β-actin expression. Sequence-specific primers were designed as follows: mouse TNF-α, 5′-GGT GCC TAT GTC TCA GCC TCT T-3′ (sense) and 5′-GCC ATA GAA CTG ATG AGA GGG A-3′ (antisense); mouse interleukin-13 (IL-13), 5′-AAC GGC AGC ATG GTA TGG AGT G-3′ (sense) and 5′-TGG GTC CTG TAG ATG GCA TTG C-3′ (antisense); mouse IL-33, 5′-CTA CTG CAT GAG ACT CCG TTC TG-3′ (sense) and 5′-AGA ATC CCG TGG ATA GGC AGA G-3′ (antisense); mouse thymic stromal lymphopoietin (TSLP), 5′-TCG AGC AAA TCG AGG ACT GTG-3′ (sense), and 5′-CAA ATG TTT TGT CGG GGA GTG A-3′ (antisense); mouse β-actin, 5′-ATG GAT GAC GAT ATC GCT C-3′ (sense) and 5′-GAT TCC ATA CCC AGG AAG G-3′ (antisense).

TEM. For transmission electron microscopy (TEM), mouse skin or cultured MEFs were fixed in buffered 4% paraformaldehyde and 2% glutaraldehyde at 4°C overnight. The samples were then suspended in 1% osmium tetroxide in 0.1 M phosphate buffer (pH 7.4) at 4°C for 1 h, dehydrated, and infiltrated with epoxy resin (Luveak 812; Nacalai Tesque). Ultrathin sections (60- to 70-nm thick) were stained with uranyl acetate and lead citrate and then analyzed by using a transmission electron microscope (model H-7650; Hitachi).

Immunoblotting. For immunoblotting, cells were lysed with lysis buffer containing 50 mM Tris-HCl (pH 7.5), 150 mM NaCl, 1% Triton X-100, and 2 mM phenylmethylsulfonyl fluoride (PMSF), a protease inhibitor cocktail (Sigma-Aldrich), and a phosphatase inhibitor cocktail (Nacalai Tesque). The lysates were centrifuged at 15,000 rpm for 20 min at 4°C, and the supernatant was used in subsequent steps. Samples were resolved by sodium dodecyl sulfate-polyacrylamide gel electrophoresis and transferred to polyvinylidene difluoride membranes. After blocking in Tris-buffered saline containing 0.1% Tween 20 and 5% (wt/vol) nonfat dry milk, the membranes were immunoblotted with the appropriate primary antibodies. The bound antibodies were visualized via enhanced chemiluminescence after incubation with horseradish peroxidase-conjugated secondary antibodies directed against mouse or rabbit IgG. Immunoblotted protein bands were visualized by using an LAS3000 or LAS4000 mini-imaging analyzer (Fujifilm).

Antibodies and reagents. Anti-HOIP, anti-HOIL-1L, anti-SHARPIN, antitubulin, and anti-β-actin antibodies have been described previously (8, 9, 13). The following antibodies were obtained from commercial sources: anti-IκBα, anti-pIκBα, anti-caspase 3, and anti-cleaved caspase 3 (Cell Signaling Technology); anti-FLAG (MBL and Santa Cruz Biotechnology); anti-myc (Millipore); anti-pNF-κB p65, antiubiquitin, and anti-glutathione *S*-transferase (anti-GST) (Santa Cruz Biotechnology); anti-TNFR1 and anti-pMLKL (Abcam); anti-TNF-α (eBioscience); and Alexa Fluor 546-conjugated secondary antibody (ThermoFisher Scientific).

Cell death analysis using the iCELLigence system. The iCELLigence real-time cell analyzer system (ACEA Biosciences) continuously measures electrical impedance of the cell population in the E-plate with a microelectronic biosensor built into the wells. A dimensionless parameter termed the cell index (CI) is derived as a relative change in measured electrical impedance, reflecting the viability of the adherent cultured cells upon stimulation with the indicated chemicals. Data were normalized to the last time point before the addition of chemicals to give the normalized

A

HOIL-1L$^{-/-}$ SHARPIN$^{+/cpdm}$× HOIL-1L$^{-/-}$ SHARPIN$^{+/cpdm}$	Mendelian frequency	Observed frequency	Number of mice
HOIL-1L $^{-/-}$ SHARPIN$^{+/+}$	25%	34%	16
HOIL-1L $^{-/-}$ SHARPIN$^{+/cpdm}$	50%	66%	31
HOIL-1L $^{-/-}$ SHARPIN$^{cpdm/cpdm}$	25%	0%	0
Total	100%	100%	47

B

	HOIL-1L$^{-/-}$ SHARPIN$^{+/+}$	HOIL-1L$^{-/-}$ SHARPIN$^{+/cpdm}$	HOIL-1L$^{-/-}$ SHARPIN$^{cpdm/cpdm}$	Total
E9.5	8	12	3	23
E10.5	15	11	7	33
E11.5	9	19	0	28
E12.5	8	10	0	18

C

HOIP$^{+/\Delta linear}$×HOIP$^{+/\Delta linear}$	Mendelian frequency	Observed frequency	Number of mice
HOIP$^{+/+}$	25%	36%	27
HOIP$^{+/\Delta linear}$	50%	64%	47
HOIP$^{\Delta linear/\Delta linear}$	25%	0%	0
Total	100%	100%	74

D

	HOIP$^{+/+}$	HOIP$^{+/\Delta linear}$	HOIP$^{\Delta linear/\Delta linear}$	Total
E9.5	13	30	10	53
E10.5	9	26	11	44
E11.5	9	30	0	39
E12.5	8	19	0	27

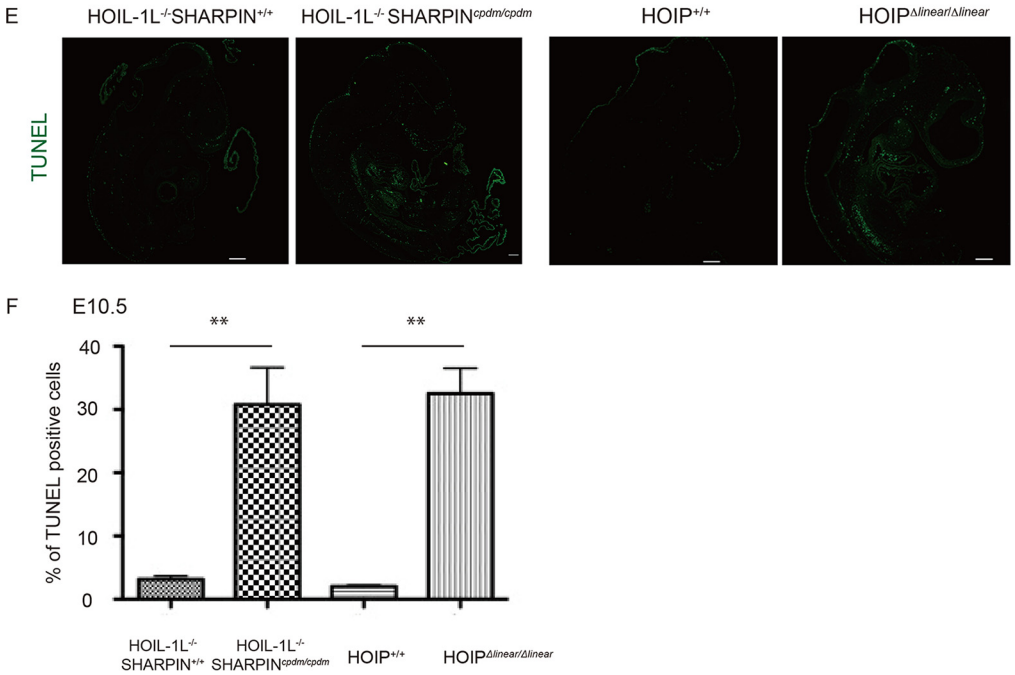

FIG 1 HOIL-1L$^{-/-}$ SHARPIN$^{cpdm/cpdm}$ and HOIP$^{\Delta linear/\Delta linear}$ mice exhibit embryonic lethality at identical gestational stages due to augmented cell death. (A and C) Quantification of genotypes of animals obtained after crossing HOIL-1L$^{-/-}$ SHARPIN$^{+/cpdm}$ (A) and HOIP$^{+/\Delta linear}$ (C) mice. Expected values according to Mendelian frequencies are indicated. (B and D) The numbers of embryos obtained at each embryonic stage (E9.5, E10.5, E11.5, and E12.5) after crossing HOIL-1L$^{-/-}$ SHARPIN$^{+/cpdm}$ (B) and HOIP$^{+/\Delta linear}$ (D) mice are shown. (E) Representative images of TUNEL staining of paraffin-sectioned embryos of the indicated genotypes at E10.5. Scale bars, 200 μm. (F) Quantification of TUNEL-positive cells at embryonic day 10.5 from paraffin-embedded sections with the indicated genotypes ($n = 3$). Data are given as the mean ± standard error of the mean (SEM). (Significance: **, $P < 0.01$.)

CI. The normalized CI is defined as the $CI_{original}/CI_{normalized\ time}$, and the delta CI is defined as the $CI_{original} + (\Delta CI_{reference} - CI_{delta\ time})$.

Generation of mutants. The open reading frames (ORFs) of mouse SHARPIN and HOIL-1L were amplified by RT-PCR. The deletion and truncated mutants listed as follows were generated from the amplified SHARPIN ORF: N-term (amino acids 1 to 162), UBL (amino acids 163 to 340), NZF (amino acids 342 to 380), ΔN-term (amino acids 163 to 380), ΔUBL (amino acids 1 to 232 and 306 to 380), and ΔNZF (amino acids 1 to 347). Chimeric SHARPIN and HOIL-1L, with interchanged NZF domains (SHARPIN NZF, amino acids 342 to 380; HOIL-1L NZF, amino acids 192 to 250), were generated via three-step PCR by using the amplified ORFs of mouse SHARPIN and HOIL-1L. The generated cDNAs were ligated to the appropriate epitope tag sequences and then cloned into the pMXs-IP retroviral mammalian expression plasmid (kindly provided by Toshio Kitamura, the Institute of Medical Science, University of Tokyo). The cpdm MEFs and HOIL-1L$^{-/-}$ SHARPIN$^{cpdm/cpdm}$ MEFs stably expressing wild type (WT), deleted, truncated, or chimeric proteins of SHARPIN or HOIL-1L were generated by using a retroviral expression system. Stable clones were selected by using 2 μg/ml puromycin (Sigma-Aldrich).

Protein expression and purification. To generate expression constructs, coding sequences for NZF proteins of the mouse HOIL-1L (amino acids 192 to 250), mouse SHARPIN (amino acids 342 to 380), and SHARPIN T351L/F352V mutants (amino acids 342 to 380) were cloned into the

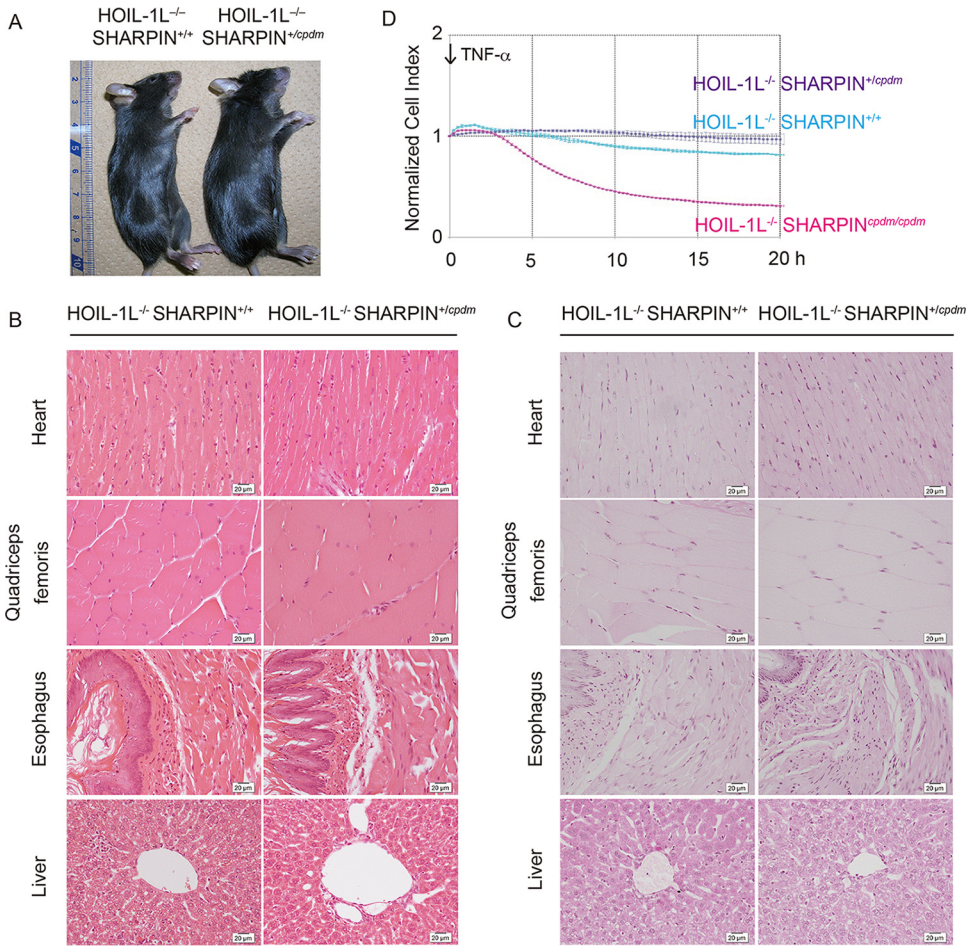

FIG 2 Reduction of SHARPIN in HOIL-1L$^{-/-}$ mice does not induce abnormal glycogen storage diseases or sensitize MEFs to TNF-α-induced cell death. (A) Representative images of HOIL-1L$^{-/-}$ SHARPIN$^{+/+}$ mice and HOIL-1L$^{-/-}$ SHARPIN$^{+/cpdm}$ mice with their littermates at 12 weeks of age. (B and C) Histological analyses of the organs commonly affected by glycogen storage diseases in human patients using H&E (B) or PAS (C) staining of mouse tissue sections from 12-week-old animals of the indicated genotypes. Representative sections ($n \geq 3$ mice) from mice of each genotype are shown. (D) The viability of MEFs obtained from mice of the indicated genotypes was continuously measured with the iCELLigence system upon stimulation with TNF-α (10 ng/ml) ($n = 3$). Data are given as the mean ± SEM.

pGEX-6p-1 vector, and the coding sequence for the NZF protein of mouse TAB2 (amino acids 665 to 693) was cloned into the pHTNHis$_6$HaloTag T7 vector (Promega) and then expressed in *Escherichia coli* [BL-21-CodonPlus(DE3)-RIPL; Agilent Technologies]. The overexpression of the GST-tagged or His$_6$Halo-tagged protein was induced by 0.5 mM isopropyl-β-D-thiogalactopyranoside (Nacalai Tesque), followed by a further 3 h of incubation at 30°C. Cells were collected by centrifugation and frozen rapidly. Cells were resuspended in buffer containing 50 mM Tris-HCl (pH 7.5), 150 mM NaCl, 1 mM dithiothreitol (Nacalai Tesque), 200 μg/ml lysozyme chloride (Nacalai Tesque), 10 μg/ml DNase (Roche Diagnostics K.K.), and 1 mM phenylmethylsulfonyl fluoride (PMSF) at 4°C for 30 min and lysed in the presence of 0.1% of Triton X-100 at 4°C for 1 h. Insoluble material was removed by centrifugation at 14,000 × *g* for 20 min at 4°C. GST- or His$_6$Halo-tagged protein was purified from the supernatant by using glutathione-Sepharose beads or Ni-nitrilotriacetic acid (Ni-NTA) beads, respectively.

GST pulldown assay. GST-fused NZF proteins derived from the HOIL-1L, SHARPIN, and SHARPIN T351L/F352V mutants (2 μg) were incubated at 4°C for 1 h with K11-, K63-, or M1-linked ubiquitin chains (1 μg) in 300 μl of buffer containing 20 mM Tris-HCl (pH 7.5), 20 μM $ZnCl_2$, 1 mM dithiothreitol, 150 mM NaCl, and 0.1% Triton X-100, followed by incubation with glutathione-Sepharose beads at 4°C for 1 h. Next, the beads were washed four times with the same buffer, boiled in sodium dodecyl sulfate sample buffer, and analyzed by immunoblotting.

Immunoprecipitation of TNFR1. cpdm MEFs with retrovirally introduced SHARPIN WT, SHARPIN-HOIL-1L NZF, SHARPIN ΔNZF, SHARPIN T351L/F352V mutant, or empty vector were treated with Flag-tagged TNF-α (ENZO Life Sciences) (1 μg/ml) for the time periods indicated in Fig. 8B to D at 37°C and lysed with lysis buffer containing 20 mM Tris-HCl (pH 7.5), 150 mM NaCl, 0.2% NP-40, 10% glycerol, 2 mM PMSF, and a protease inhibitor cocktail (Sigma-Aldrich), followed by centrifugation at 10,000 ×*g* for 20 min at 4°C. The TNFR1 complex was immunoprecipitated by 30 μg of FLAG M2 antibody coupled with Dynabeads protein G (Novex by Life Technologies) at 4°C for 75 min. The precipitates were washed five times with the same lysis buffer. The TNFR1 complex was eluted with 400 ng/μl of 3×FLAG peptide (Sigma) in 22.5 μl of phosphate-buffered saline at 37°C for 40 min and then analyzed by immunoblotting.

Pulldown assay with His$_6$Halo-fused TAB2 NZF. His$_6$Halo-fused NZF derived from mouse TAB2 (5 μg) was incubated with 30 μl of equilibrated Magne HaloTag beads (Promega) at 4°C for 1 h in 300 μl of buffer containing 20 mM Tris-HCl (pH 7.5), 20 μM $ZnCl_2$, 1 mM dithiothreitol, 150 mM NaCl, and 0.1% Triton X-100 for Halo-fused TAB2 NZF to bind with Magne HaloTag beads, followed by extensive washing three times

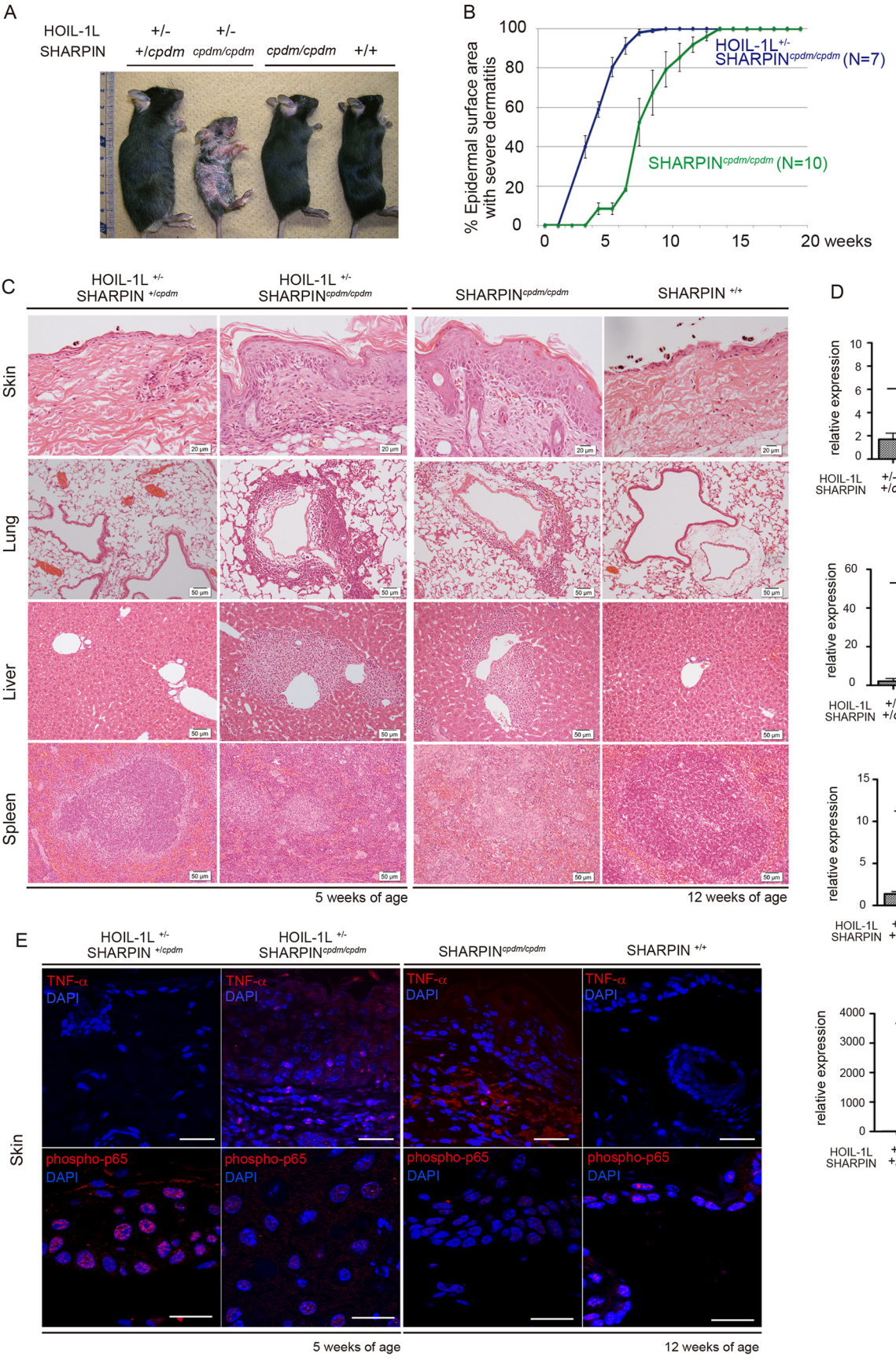
A
HOIL-1L
SHARPIN
+/-
+/cpdm
+/-
cpdm/cpdm
cpdm/cpdm
+/+
B
% Epidermal surface area with severe dermatitis
100
80
60
40
20
0
0
5
10
15
20 weeks
HOIL-1L+/- SHARPINcpdm/cpdm (N=7)
SHARPINcpdm/cpdm (N=10)
C
HOIL-1L +/- SHARPIN +/cpdm
HOIL-1L +/- SHARPINcpdm/cpdm
SHARPINcpdm/cpdm
SHARPIN +/+
Skin
Lung
Liver
Spleen
5 weeks of age
12 weeks of age
D
TNF-α
IL-13
IL-33
TSLP
5 w
12 w
relative expression
HOIL-1L SHARPIN
+/- +/cp
+/- cp/cp
+/+ or +/cp
cp/cp
E
TNF-α
DAPI
phospho-p65
DAPI
Skin
5 weeks of age
12 weeks of age

with buffer containing 20 mM Tris-HCl (pH 7.5), 150 mM NaCl, 0.2% NP-40, and 10% glycerol. The TNFR1 complex eluted as described above was incubated with Magne HaloTag beads capturing Halo-TAB2 NZF in 300 μl of buffer containing 20 mM Tris-HCl (pH 7.5), 150 mM NaCl, 0.2% NP-40, and 10% glycerol at 4°C for 4 h. The precipitates were washed five times with the same buffer, boiled in sodium dodecyl sulfate sample buffer, and analyzed by immunoblotting.

Statistical analysis. Statistical significance was analyzed by using an unpaired Student *t* test with Prism 6 (GraphPad Software).

RESULTS

HOIL-1$^{-/-}$ SHARPIN$^{cpdm/cpdm}$ mice and HOIP$^{\Delta linear/\Delta linear}$ mice are both embryonic lethal at the same midgestational stage. To investigate the coordinate and distinct functions of the two accessory subunits in LUBAC, we intercrossed mice lacking either SHARPIN or HOIL-1L. First, we examined the phenotype of mice losing both HOIL-1L and SHARPIN alleles. HOIL-1L$^{-/-}$ SHARPIN$^{cpdm/cpdm}$ mice were embryonic lethal (Fig. 1A) and died at approximately E10.5 (Fig. 1B), similar to HOIP mutant mice lacking ubiquitin ligase activity (Fig. 1C and D). Because increased programmed cell death underlies embryonic lethality in HOIP$^{-/-}$ mice at E10.5 (16), we next examined TUNEL staining as a marker of dying cells in HOIL-1L$^{-/-}$ SHARPIN$^{cpdm/cpdm}$ and HOIP$^{\Delta linear/\Delta linear}$ mice. Consequently, TUNEL-positive cells increased to equivalent levels at E10.5 in both HOIL-1L$^{-/-}$ SHARPIN$^{cpdm/cpdm}$ and HOIP$^{\Delta linear/\Delta linear}$ mice relative to their littermate controls (Fig. 1E and F). Therefore, loss of the two LUBAC accessory subunits apparently downregulated the ligase activity of the complex to a level comparable to that which occurs upon loss of the HOIP catalytic subunit. Moreover, the HOIL-1L/SHARPIN-mediated loss of linear ubiquitination activity led to enhanced programmed cell death and embryonic lethality at the same gestational age at which HOIP$^{-/-}$ mice die (16). These gross phenotypical inspections confirm that the three LUBAC subunits are the main functional constituents of LUBAC.

HOIL-1L reduction increases the severity of inflammatory diseases without inducing any additional phenotype in SHARPIN$^{cpdm/cpdm}$ mice. We next focused on the molecular mechanism of chronic inflammation provoked by the loss of SHARPIN. To do so, the offspring of intercrossed mice lacking SHARPIN or HOIL-1L were investigated by using a number of parameters. Introduction of one SHARPIN-null cpdm allele into HOIL-1L$^{-/-}$ mice (HOIL-1L$^{-/-}$ SHARPIN$^{+/cpdm}$ mice) failed to induce any characteristic inflammatory phenotype or metabolic disorders (e.g., amylopectinosis) that have been previously reported in humans deficient in HOIL-1L (Fig. 2A to C) (30). Surprisingly, however, deletion of one allele of HOIL-1L in cpdm mice (HOIL-1L$^{+/-}$ SHARPIN$^{cpdm/cpdm}$ mice) accelerated the onset and exacerbated the severity of cpdm diseases. For instance, inflammatory changes were detected in mice as young as 5 weeks of age, at which time cpdm mice do not usually exhibit any obvious phenotype (20) (Fig. 3A and B). However, the organs affected in HOIL-1L$^{+/-}$ SHARPIN$^{cpdm/cpdm}$ mice were limited to the skin, lung, liver, and spleen, i.e., the same organs as those affected in cpdm mice (Fig. 3C). Moreover, the histopathological changes observed in the 5-week-old HOIL-1L$^{+/-}$ SHARPIN$^{cpdm/cpdm}$ mice and the types and levels of upregulated transcripts of inflammatory cytokines in the skin were almost identical to those observed in 12-week-old SHARPIN$^{cpdm/cpdm}$ mice (Fig. 3C and D). Immunohistochemical analyses of the skin confirmed increased TNF-α production presumably from a number of infiltrated inflammatory cells in 5-week-old HOIL-1L$^{+/-}$ SHARPIN$^{cpdm/cpdm}$ and 12-week-old SHARPIN$^{cpdm/cpdm}$ mice (Fig. 3E) (31). Phosphorylation of the p65 subunit of NF-κB is known to be a reliable marker of NF-κB activation (32). Phospho-p65 staining revealed the attenuated NF-κB activation in 5-week-old HOIL-1L$^{+/-}$ SHARPIN$^{cpdm/cpdm}$ and 12-week-old SHARPIN$^{cpdm/cpdm}$ mice (Fig. 3E). These results suggest that the loss of SHARPIN is critical for the pathogenesis of chronic inflammation by increasing the amount of inflammatory cytokines and attenuated TNF receptor signaling in the skin.

A prevailing hypothesis for the pathogenesis of inflammation in cpdm mice is that the loss of SHARPIN strongly sensitizes individuals to TNF-α-induced programmed cell death (14, 15, 17, 18). In support of this idea, our transmission electron microscopy (TEM) observations of cpdm mice revealed a subpopulation of keratinocytes displaying the characteristic morphology of both apoptosis and necroptosis (Fig. 4A). Moreover, immunohistochemical analyses showed positive signals of cleaved caspase 3 and phosphorylated mixed-lineage kinase domain-like (pMLKL), the specific markers of apoptosis and necroptosis, respectively, in the epidermis (Fig. 4B). These observations indicated that apoptosis and necroptosis, which are two types of programmed cell death induced by various stimuli, including TNF-α, could occur in cpdm mouse skin (33). Additionally, mouse embryonic fibroblasts (MEFs) obtained from cpdm mice exhibited the characteristic morphological features as well as specific markers of apoptosis and necroptosis upon stimulation with TNF-α (Fig. 4C and D). Furthermore, necrostatin-1, which specifically inhibits the kinase activity of RIP1 to block both apoptosis and necroptosis upon TNF-α stimulation (34), effectively rescued cpdm MEFs from TNF-α-induced cell death (Fig. 4E). Hence, loss of SHARPIN sensitizes cpdm mice to TNF-α-induced programmed cell death, in keeping with the purported inflammogenic nature of SHARPIN deficiency (35).

We have shown that the introduction of one cpdm allele of SHARPIN in HOIL-1L KO mice did not induce any overt phenotypes (Fig. 2A to C). Considering that MEFs obtained from HOIL-1L$^{-/-}$ SHARPIN$^{+/cpdm}$ mice were not sensitized to TNF-α-mediated cell death (Fig. 2D), these results collectively indicate that at least

FIG 3 Deletion of one allele of HOIL-1L in cpdm mice exacerbates cpdm-related disease symptoms without inducing additional phenotypes. (A) Macroscopic appearance of mice of the indicated genotypes at 5 weeks of age. (B) The percentage of severely affected epidermal surface area of mice of the indicated genotypes ($n = 7$ to 10) was measured weekly. Data are given as the mean ± SEM. (C) Histological analysis using H&E staining of skin, lung, liver, and spleen sections of the HOIL-1L$^{+/-}$ SHARPIN$^{+/cpdm}$ and HOIL-1L$^{+/-}$ SHARPIN$^{cpdm/cpdm}$ mice at 5 weeks of age (left two panels) and SHARPIN$^{+/+}$ and SHARPIN$^{cpdm/cpdm}$ mice at 12 weeks of age (right two panels). Representative sections ($n \geq 3$ mice) from mice of each genotype are shown. (D) RT-PCR analysis of the expression levels of inflammatory cytokines (TNF-α, IL-13, IL-33, and thymic stromal lymphopoietin [TSLP]) in samples of dorsal skin from mice of the indicated genotypes and ages are shown ($n = 5$ or 6). cp, cpdm. β-Actin was used as an internal control. Data are given as the mean ± SEM. (Significance: *, $P < 0.05$; **, $P < 0.01$; ***, $P < 0.001$). (E) Immunohistochemical analyses for TNF-α and the phospho-p65 component of NF-κB from samples of dorsal skin derived from mice of the indicated genotypes and ages. Nuclei are stained with DAPI (blue), and TNF-α and phospho-p65 are shown in red. Scale bars, 20 μm.

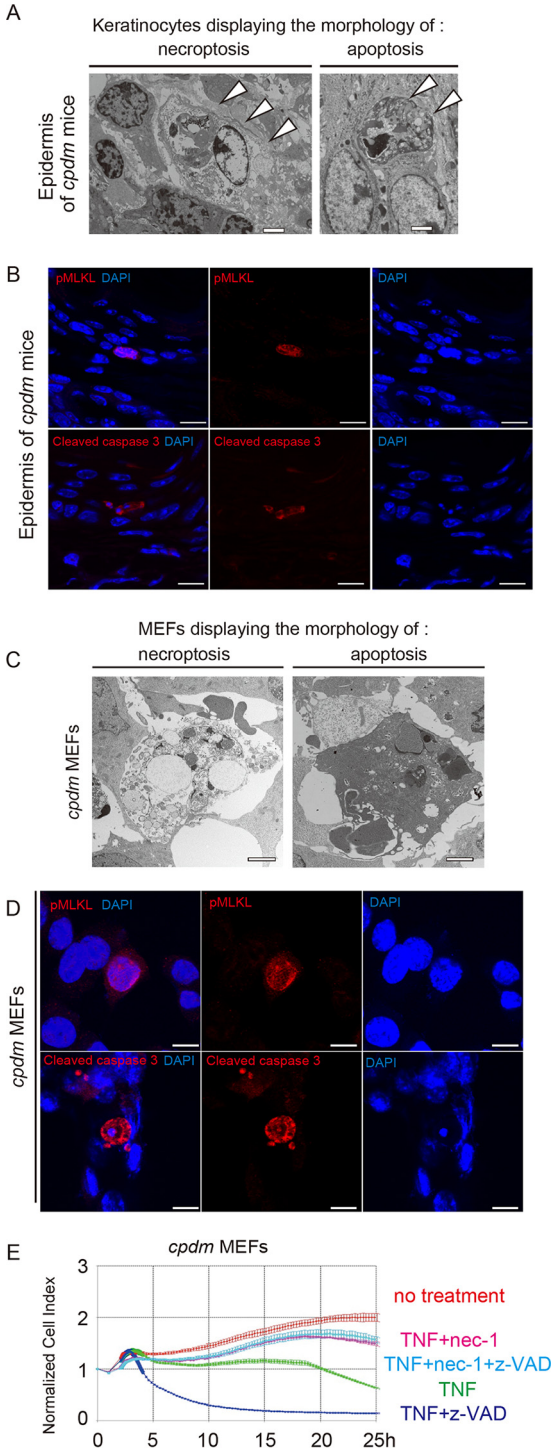

FIG 4 Loss of SHARPIN induces both apoptosis and necroptosis upon TNF-α stimulation. (A) The epidermis of cpdm mice at 8 weeks of age was inspected by using a transmission electron microscope (TEM). The arrowheads indicate keratinocytes displaying the characteristic morphology of necroptosis (left panel) and apoptosis (right panel). Scale bars, 2 μm. Representative data ($n \geq 3$ mice) are shown. (B) Immunohistochemical analysis of the phosphorylated form of mixed-lineage kinase domain-like (pMLKL) and cleaved caspase 3 on the epidermis of cpdm mice at 12 weeks of age. Scale bars, 10 μm. Nuclei are stained with DAPI (blue), and pMLKL and cleaved caspase 3 are shown in red. (C) Morphological changes of cpdm MEFs were inspected by TEM following stimulation with TNF-α (10 ng/ml). Scale bars, 3 μm. (D) Immunocytochemical analyses for pMLKL and cleaved caspase 3 on cpdm MEFs stimulated with TNF-α (10 ng/ml) for 8 h. Nuclei are stained with DAPI (blue), and cleaved caspase 3 or phospho-MLKL is shown in red. Scale bars, 10 μm. (E) The viability of MEFs obtained from cpdm mice was continuously measured with the iCELLigence system upon treatment with TNF-α (10 ng/ml), necrostatin-1 (nec-1) (50 μM), and/or z-VAD (20 μM), as indicated ($n = 3$). Data are given as the mean ± SEM.

one SHARPIN allele is sufficient for the inhibition of TNF-α-induced cell death.

HOIL-1L reduction further impairs LUBAC functions in SHARPIN$^{cpdm/cpdm}$ MEFs. In addition to the essential roles of SHARPIN in antagonizing the onset of inflammatory disease, our intercrossing analyses with HOIL-1L$^{-/-}$ and cpdm mice revealed that HOIL-1L reduction in SHARPIN$^{cpdm/cpdm}$ animals increased the severity but not the characteristic features of cpdm disease symptoms (Fig. 3). Moreover, deletion of HOIL-1L in cpdm mice resulted in embryonic lethality (Fig. 1A). In other words, the amount of HOIL-1L present seems to be critical for the gravity of the disease. Therefore, we next evaluated the impact of the number of HOIL-1L loci in SHARPIN$^{cpdm/cpdm}$ MEFs on HOIP expression levels as an indicator of LUBAC content, because most of the HOIP protein in a cell exists in the LUBAC complex (8).

Figure 5A shows an inverse correlation between HOIP expression and the number of WT HOIL-1L loci in SHARPIN$^{cpdm/cpdm}$ MEFs, where HOIP was nearly depleted in MEFs lacking both WT HOIL-1L and SHARPIN. Consistent with the functions of residual LUBAC, the smaller the amount of HOIP present, the lower the extent of TNF-α-mediated phosphorylation and degradation of IκBα (a measure of canonical NF-κB activation) (Fig. 5B). Furthermore, loss of both HOIL-1L and SHARPIN resulted in defective activation of NF-κB in HOIL-1L$^{-/-}$ SHARPIN$^{cpdm/cpdm}$ MEFs, as was also observed in HOIP$^{\Delta linear/\Delta linear}$ MEFs (Fig. 5C).

The same tendency was found for LUBAC-mediated protection against TNF-α-mediated cell death and cleavage of caspase 3, a hallmark of the execution of apoptosis. As HOIL-1L was reduced in SHARPIN$^{cpdm/cpdm}$ MEFs, the cells became more sensitized to TNF-α-induced cell death (Fig. 5D to H), and loss of both SHARPIN and HOIL-1L resulted in the same cell death sensitivity as that caused by losing the ubiquitin ligase activity of HOIP (Fig. 5F to H). Although the loss of one HOIL-1L allele augmented TNF-α-mediated cell death, necrostatin-1, but not z-VAD (pancaspase inhibitor), effectively protected HOIL-1L$^{+/-}$ SHARPIN$^{cpdm/cpdm}$ MEFs from death, as was the case for cpdm MEFs (Fig. 4E and 5I). However, in addition to necrostatin-1, z-VAD was required for effectively protecting HOIL-1L$^{-/-}$ SHARPIN$^{cpdm/cpdm}$ and HOIP$^{\Delta linear/\Delta linear}$ MEFs from death (Fig. 5J and K). These findings confirm that loss of one HOIL-1L allele did not affect the types of programmed cell death induced by loss of SHARPIN and implies that the residual ligase activity of LUBAC may have additional roles in cell death protection.

SHARPIN UBL and NZF domains protect against TNF-α-induced cell death. To dissect the molecular mechanisms by which loss of SHARPIN sensitizes cells to programmed death, we generated SHARPIN mutants lacking several functional domains (Fig. 6A) and retrovirally introduced the mutants into cpdm MEFs. Consequently, SHARPIN mutants lacking the UBL domain (N-term, NZF, and ΔUBL SHARPIN) failed to rescue cpdm MEFs from TNF-α-induced cell death, whereas SHARPIN mutants containing the UBL domain (ΔN-term, ΔNZF, and UBL

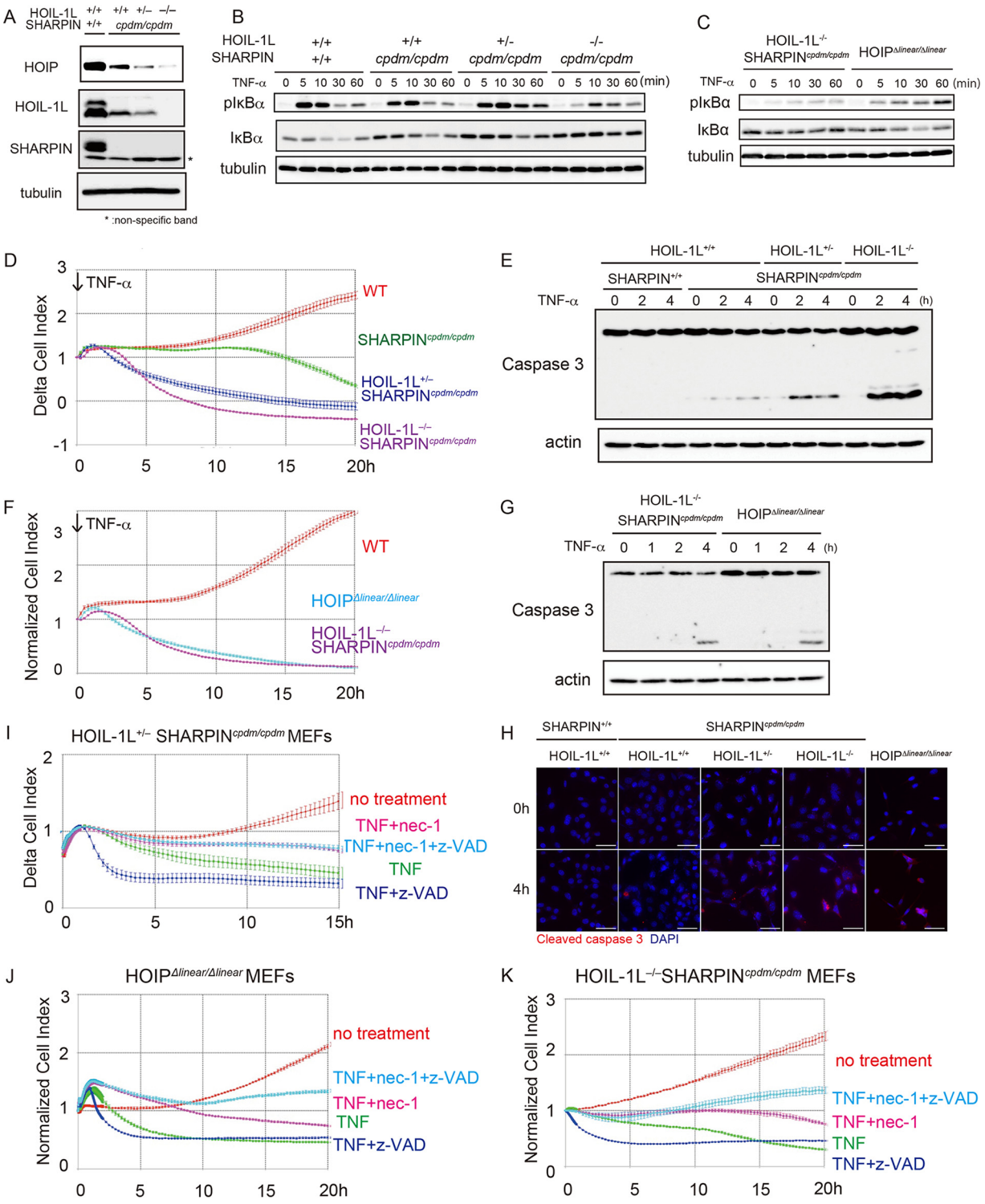

FIG 5 HOIL-1L reduction in SHARPIN$^{cpdm/cpdm}$ MEFs results in impaired stability of HOIP, NF-κB activation, and sensitization to programmed cell death. (A) Immunoblot analysis of the LUBAC components in whole-cell lysates (WCL) from MEFs with the indicated genotypes. (B and C) Immunoblot analysis of the indicated proteins in WCL from MEFs with the indicated genotypes following TNF-α stimulation (10 ng/ml) for various periods of time. (D and F) The viability of MEFs obtained from mice with the indicated genotypes was continuously measured with the iCELLigence system by using a real-time cell analyzer upon stimulation with TNF-α (10 ng/ml) ($n = 3$). Data are given as the mean ± SEM. (E and G) Immunoblot analysis of the indicated proteins in WCL from MEFs with the indicated genotypes following stimulation with TNF-α (10 ng/ml). (H) Immunocytochemical analyses for cleaved caspase 3 on MEFs with the indicated genotypes upon TNF-α stimulation (10 ng/ml) for the indicated time periods. Nuclei are stained with DAPI (blue), and cleaved caspase 3 is shown in red. Scale bars, 50 μm. (I to K) The viability of MEFs obtained from HOIL-1L$^{+/-}$ SHARPIN$^{cpdm/cpdm}$ mice was continuously measured with the iCELLigence system upon treatment with TNF-α (10 ng/ml), necrostatin-1 (nec-1) (50 μM), and/or z-VAD (20 μM), as indicated ($n = 3$). Data are given as the mean ± SEM.

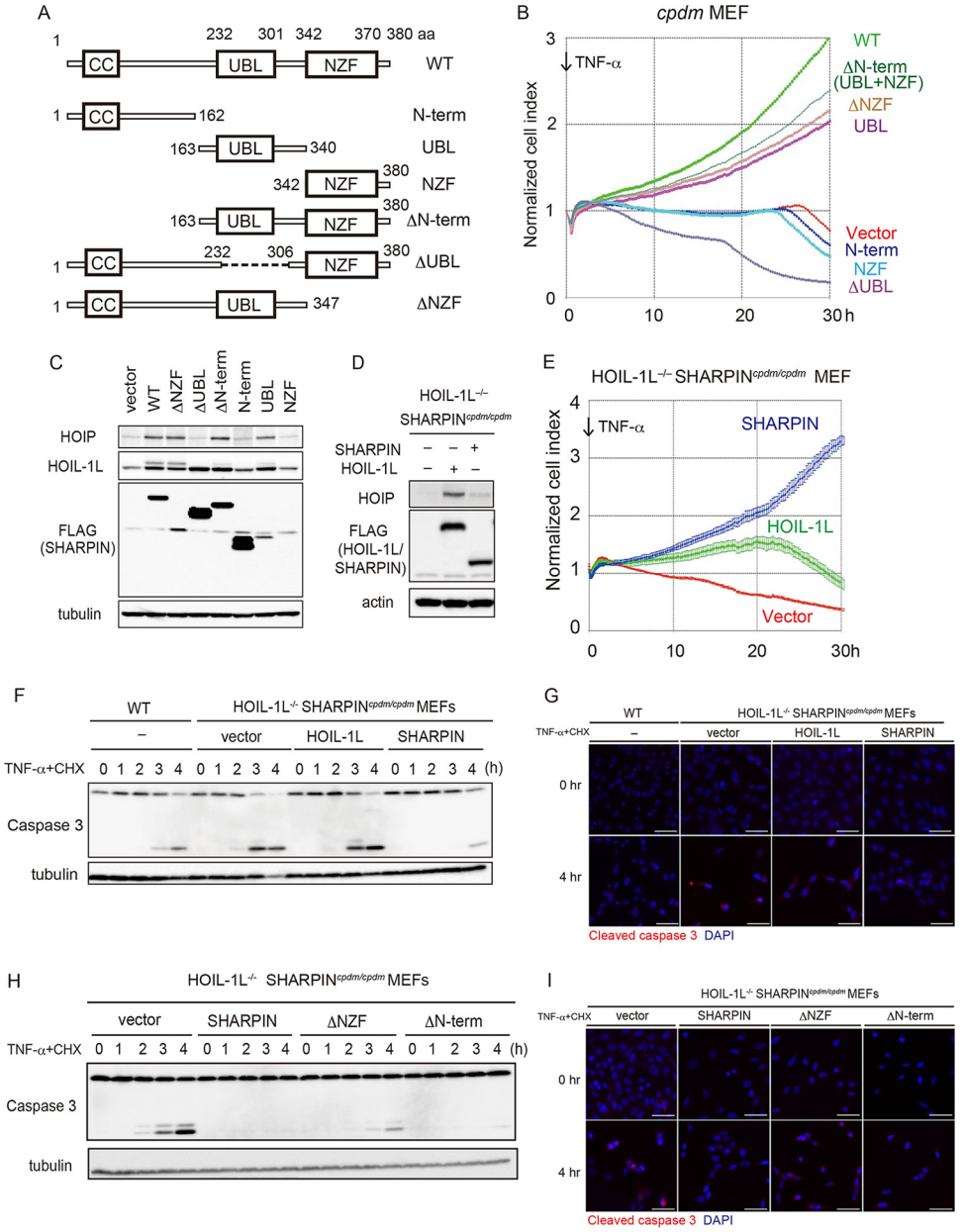

FIG 6 Restoration of HOIP levels through the SHARPIN UBL domain antagonizes programmed cell death in cpdm MEFs upon TNF-α stimulation. (A) Schematic representation of WT SHARPIN and SHARPIN mutants (CC, coiled-coil; UBL, ubiquitin-like; NZF, Npl4 zinc finger). (B) cpdm MEFs expressing the indicated proteins were treated with TNF-α (10 ng/ml). The viability of the MEFs was continuously measured with the iCELLigence system ($n = 2$). Data are given as the means of results for duplicate samples. (C) Immunoblot analysis of LUBAC components in whole-cell lysates (WCL) from cpdm MEFs infected with the indicated FLAG-tagged SHARPIN mutants. (D) Immunoblot analysis of LUBAC components in WCL from HOIL-1L$^{-/-}$ SHARPIN$^{cpdm/cpdm}$ MEFs infected with FLAG-tagged SHARPIN, HOIL-1L, or empty vector. (E) The viability of HOIL-1L$^{-/-}$ SHARPIN$^{cpdm/cpdm}$ MEFs infected with the indicated proteins or empty vector was continuously measured with the iCELLigence system following stimulation with 10 ng/ml TNF-α ($n = 3$). Data are given as the mean ± SEM. (F and H) Immunoblot analysis of the indicated proteins in WCL from WT MEFs or HOIL-1L$^{-/-}$ SHARPIN$^{cpdm/cpdm}$ MEFs infected with HOIL-1L, SHARPIN, or empty vector (F) and HOIL-1L$^{-/-}$ SHARPIN$^{cpdm/cpdm}$ MEFs infected with WT SHARPIN, SHARPIN mutants (ΔNZF and ΔN-term), or empty vector (H) following stimulation with TNF-α (10 ng/ml) in the presence of CHX (20 μg/ml). (G and I) Immunocytochemical analyses for cleaved caspase 3 on WT MEFs or HOIL-1L$^{-/-}$ SHARPIN$^{cpdm/cpdm}$ MEFs infected with HOIL-1L, SHARPIN, or empty vector (G) and HOIL-1L$^{-/-}$ SHARPIN$^{cpdm/cpdm}$ MEFs infected with WT SHARPIN, SHARPIN mutants (ΔNZF and ΔN-term), or empty vector (I) following stimulation with TNF-α (10 ng/ml) in the presence of CHX (20 μg/ml). Nuclei are stained with DAPI (blue), and cleaved caspase 3 is shown in red. Scale bars, 50 μm.

SHARPIN) or WT SHARPIN increased cell survival in the presence of the cytokine (Fig. 6B). Introduction of WT SHARPIN or its UBL domain-containing mutants into cpdm MEFs significantly restored the amount of endogenous HOIP protein (Fig. 6C), thereby restoring LUBAC content (13). Nevertheless, although HOIL-1L overexpression increased endogenous HOIP content to even a greater degree than SHARPIN overexpression did in MEFs lacking both HOIL-1L and SHARPIN (HOIL-1L$^{-/-}$

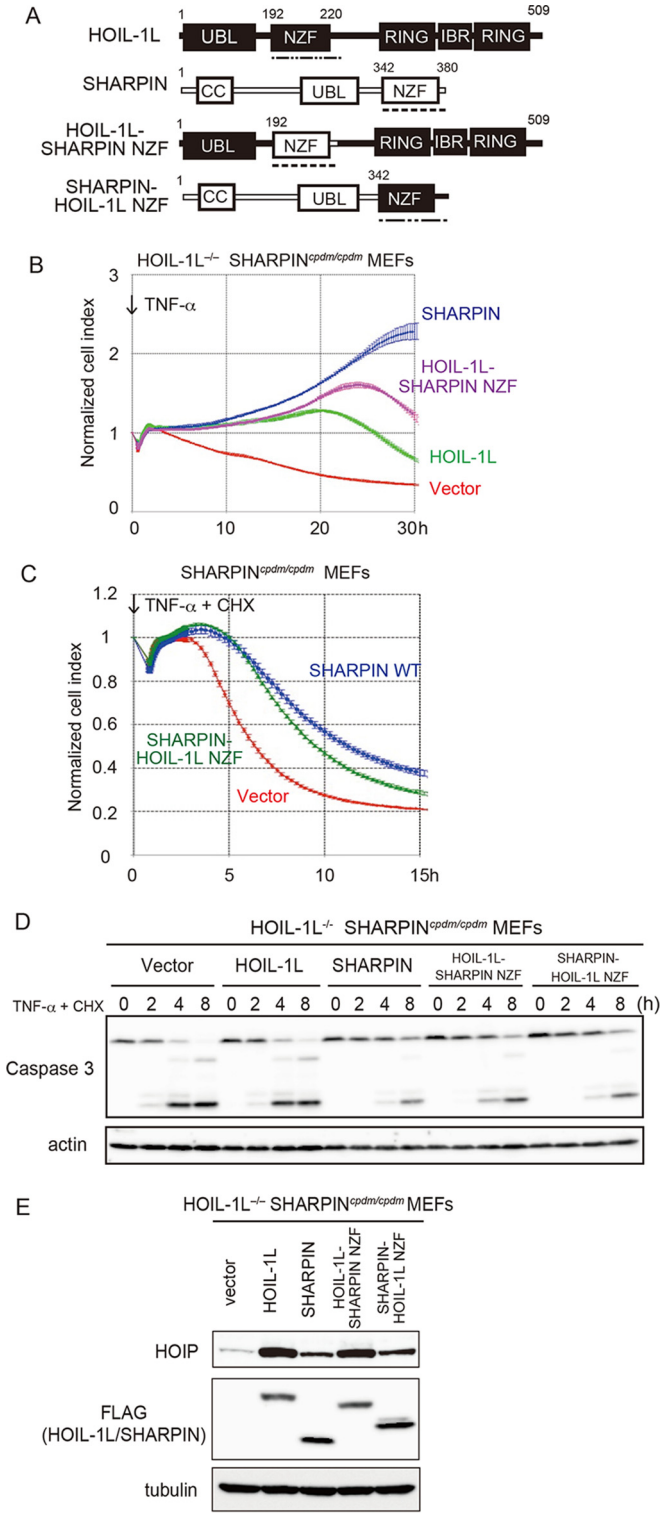

FIG 7 The SHARPIN NZF domain is required for effective protection against TNF-α-induced programmed cell death. (A) Schematic representation of SHARPIN, HOIL-1L, and SHARPIN or HOIL-1L mutants in which the NZF domains were exchanged. (B) The viability of HOIL-1L$^{-/-}$ SHARPIN$^{cpdm/cpdm}$ MEFs expressing the indicated proteins (constructs introduced by retroviral infection) was continuously measured with the iCELLigence system following stimulation with TNF-α (10 ng/ml) ($n = 3$). (C) The viability of SHARPIN$^{cpdm/cpdm}$ MEFs expressing the indicated proteins (constructs introduced by retroviral infection) was continuously measured with the iCELLigence system following stimulation with TNF-α (10 ng/ml) in the presence of CHX (20 μg/ml) ($n = 3$). Data are given as the mean ± SEM. (D) Immunoblot analysis of the indicated proteins in whole-cell lysates (WCL) from HOIL-1L$^{-/-}$ SHARPIN$^{cpdm/cpdm}$ MEFs expressing HOIL-1L, SHARPIN, HOIL-1L-SHARPIN NZF, SHARPIN-HOIL-1L NZF, or empty vector following stimulation with TNF-α (3 ng/ml) in the presence of CHX (20 μg/ml). (E) Immunoblot analysis of LUBAC components in WCL from HOIL-1L$^{-/-}$ SHARPIN$^{cpdm/cpdm}$ MEFs infected with FLAG-tagged SHARPIN, HOIL-1L, HOIL-1L-SHARPIN NZF, SHARPIN-HOIL-1L NZF, or empty vector.

SHARPIN$^{cpdm/cpdm}$ MEFs) (Fig. 6D), HOIL-1L was not as effective as SHARPIN in protecting the HOIL-1L$^{-/-}$ SHARPIN$^{cpdm/cpdm}$ MEFs from TNF-α-induced cell death (Fig. 6E to G). Therefore, SHARPIN apparently plays important roles in suppressing programmed cell death, which is distinct from its role in stabilizing LUBAC via its UBL domain.

Notably, among the mutants containing UBL, the SHARPIN mutants lacking the NZF domain protected cpdm MEFs less efficiently from TNF-α-induced cell death than those containing NZF. This was the case even though HOIP was expressed at equivalent levels among the assorted engineered MEFs (Fig. 6B, C, H, and I), which implies that the NZF domain of SHARPIN plays a significant role in protecting programmed cell deaths. To disclose the functional significance of the SHARPIN NZF domain, we next generated chimeric HOIL-1L or SHARPIN proteins in which the NZF domains were exchanged (Fig. 7A). The chimeric HOIL-1L protein containing the SHARPIN NZF domain (HOIL-1L-SHARPIN NZF) protected HOIL-1L$^{-/-}$ SHARPIN$^{cpdm/cpdm}$ MEFs more effectively than WT HOIL-1L, suggesting that the SHARPIN NZF domain is indeed involved in an efficient defense against TNF-α-mediated programmed cell death (Fig. 7B). We then treated the cells with cycloheximide (CHX), an inhibitor of translation, together with TNF-α to eliminate the prosurvival effects of NF-κB target gene products. In this way, we could evaluate the impact of LUBAC on the regulation of cell death separate from NF-κB activation. The chimeric SHARPIN protein containing the HOIL-1L NZF domain (SHARPIN-HOIL-1L NZF) did not protect cpdm MEFs from cell death as efficiently as WT SHARPIN, confirming that the SHARPIN NZF more actively safeguards against cell death than the HOIL-1L NZF (Fig. 7C to E).

The ubiquitin-binding activity of SHARPIN NZF is involved in LUBAC recruitment to the activated TNFR complex to effectively activate the canonical NF-κB pathway and protect against programmed cell death. Considering that NZF domains have ubiquitin-binding activity (21) and that the HOIL-1L NZF domain specifically recognizes M1-linked linear ubiquitin chains (19), we hypothesized that the functional differences between the SHARPIN and HOIL-1L NZFs might be attributed to differential binding to different types of ubiquitin chains. To investigate the binding of the SHARPIN and HOIL-1L NZFs to ubiquitin chains with different linkages, we purified the NZF domains of both subunits fused to the C terminus of glutathione *S*-transferase (GST) and performed pulldown assays with K11-, K63-, and M1-linked ubiquitin chains, all of which are shown to exist in the activated TNFR complex (1, 36). While the HOIL-1L NZF domain specifically recognized M1-linked linear ubiquitin chains, as documented previously (19), the SHARPIN NZF domain bound to both K63- and M1-linked ubiquitin chains (Fig. 8A). Neither NZF domain associated with K11-linked ubiquitin chains (Fig. 8A).

We then generated a SHARPIN NZF mutant in which Thr 351

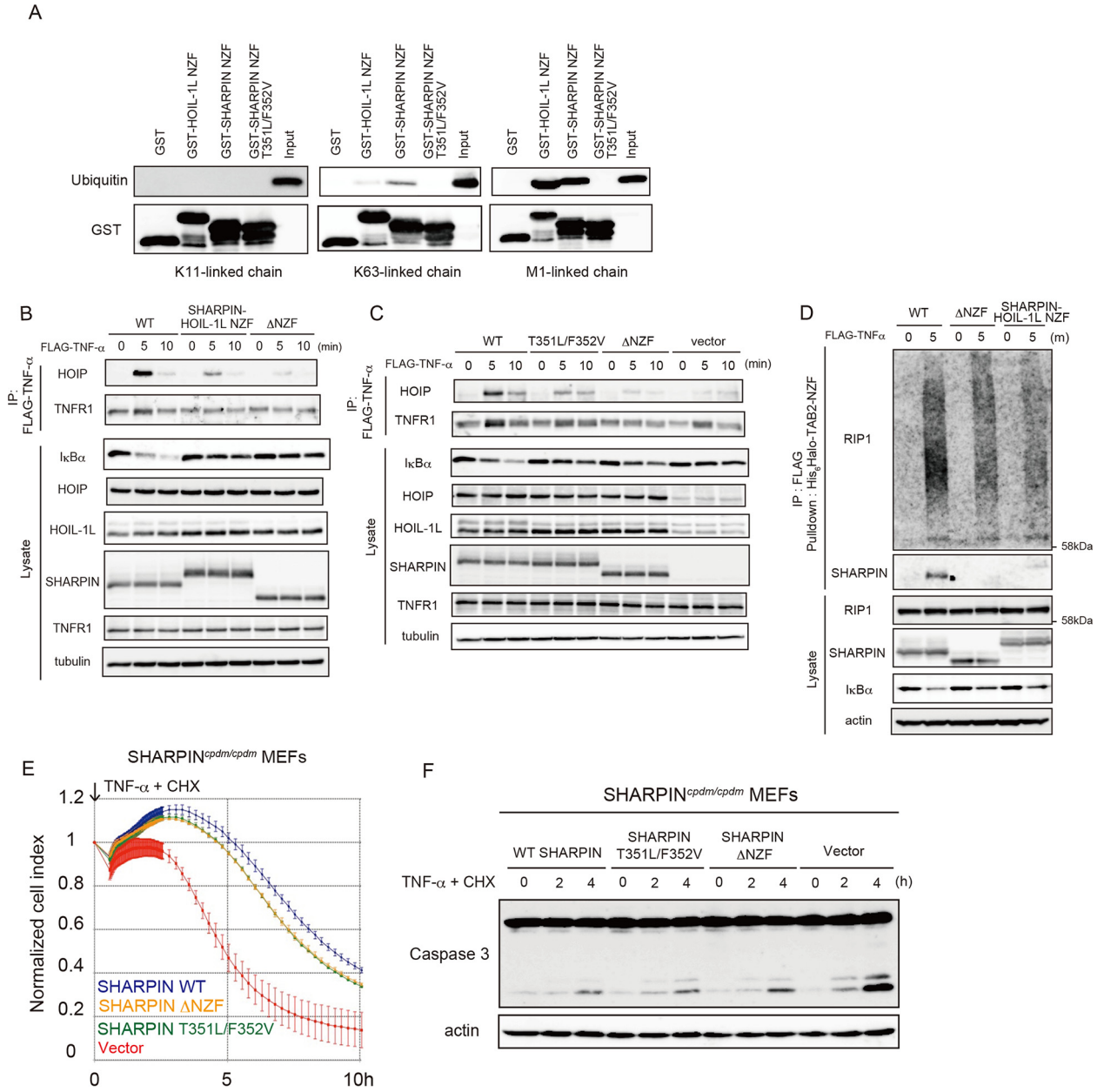

FIG 8 SHARPIN NZF domain-mediated recognition of K63-linked ubiquitin chains contributes to the recruitment of LUBAC to the activated TNFR complex to activate canonical NF-κB and protect against programmed cell death. (A) The purified NZF protein of GST-fused HOIL-1L, SHARPIN, and the SHARPIN T351L/F352V mutant was incubated with ubiquitin chains with the indicated linkages, followed by pulldown with glutathione-Sepharose beads. Ubiquitin or GST was immunoblotted as indicated. (B and C) SHARPIN$^{cpdm/cpdm}$ MEFs expressing the indicated myc-tagged-constructs (ΔNZF, SHARPIN-HOIL-1L NZF, SHARPIN T351L/F352V, or empty vector) were stimulated with FLAG-tagged TNF-α (1 μg/ml) for the indicated periods of time. Whole-cell lysates (WCL) were immunoprecipitated (IP) with anti-FLAG antibody and immunoblotted as indicated. (D) The purified His_6Halo-tagged TAB2 NZF protein was incubated with immunoprecipitated TNFR complex, followed by pulldown with Magne HaloTag beads. The precipitate was immunoblotted as indicated. (E) The viability of SHARPIN$^{cpdm/cpdm}$ MEFs expressing the indicated proteins was continuously measured with the iCELLigence system following stimulation with TNF-α (1 ng/ml) in the presence of CHX (20 μg/ml) ($n = 3$). Data are given as the mean ± SEM. (F) Immunoblot analysis of the indicated proteins in WCL from SHARPIN$^{cpdm/cpdm}$ MEFs expressing WT SHARPIN, SHARPIN mutants (T351L/F352V and ΔNZF), or empty vector following stimulation with TNF-α (10 ng/ml) in the presence of CHX (20 μg/ml).

and Phe 352, critical amino acids for ubiquitin recognition by the NZF, were replaced with Leu and Val (T351L/F352V), respectively (21). The T351L/F352V mutation in the SHARPIN NZF domain abolished ubiquitin binding (Fig. 8A), demonstrating the specificity of the experiment. The results shown in Fig. 8A suggest that differences in the affinity for K63-linked ubiquitin chains yield functional differences in the SHARPIN and HOIL-1L NZF domains.

Because ubiquitin chains conjugated to the activated TNFR complex reportedly provide recruitment platforms for signaling molecules (1), we examined whether the SHARPIN NZF domain crucially participates in the recruitment of LUBAC to the com-

plex. To do this, we immunoprecipitated the TNFR complex activated with FLAG-tagged TNF-α from cpdm MEFs with retrovirally introduced WT SHARPIN or various myc-tagged SHARPIN mutants (SHARPIN-HOIL-1L NZF, ΔNZF, or SHARPIN T351L/F352V). We then evaluated the amount of LUBAC in the activated TNFR complex. The amount of LUBAC subunits in the TNFR complex was profoundly reduced in cpdm MEFs expressing SHARPIN lacking the NZF domain (ΔNZF) or SHARPIN containing the HOIL-1L NZF (SHARPIN-HOIL-1L NZF) relative to that in MEFs expressing WT SHARPIN. Thus, the SHARPIN NZF, but not the HOIL-1L NZF, is required for LUBAC recruitment (Fig. 8B). Canonical NF-κB activation assessed by IκBα degradation was also impaired in these mutants, suggesting that the proper recruitment of LUBAC to the TNFR complex is an important step in the NF-κB cascade (Fig. 8B).

Finally, LUBAC recruitment was markedly impaired in the ubiquitin-binding-defective SHARPIN NZF mutant (T351L/F352V), in a way similar to that of the ΔNZF mutant (Fig. 8C). NF-κB activation was also compromised in cells expressing SHARPIN T351L/F352V or SHARPIN ΔNZF (Fig. 8C). To further verify the *in vivo* association of the K63-linked ubiquitin chains with the NZF domain of SHARPIN, the activated TNFR complex, which was immunoprecipitated from cpdm MEFs, retrovirally reconstituted with SHARPIN WT, SHARPIN ΔNZF, or chimeric SHARPIN whose NZF domain is exchanged with HOIL-1L NZF, was pulled down with purified TAB2 NZF fused with the His_6Halo tag (His_6Halo-TAB2 NZF), which is shown to interact with K63-linked ubiquitin chains with high specificity (37). RIP1 is known to be modified with several ubiquitin chains, including K63-linked ubiquitin chains, by some ubiquitin ligases such as cellular inhibitor of apoptosis proteins (cIAPs) upon TNF-α stimulation, and RIP1 ubiquitination precedes the recruitment of LUBAC to the activated TNFR complex (10). Since ubiquitinated RIP1 is pulled down with His_6Halo-TAB2 NZF, the activated TNFR complex purified from cells expressing SHARPIN WT or any of the above-described SHARPIN mutants contains K63-linked ubiquitin chains. However, WT SHARPIN, but not SHARPIN ΔNZF or SHARPIN-HOIL-1L NZF, could be detected in the precipitates of His_6Halo-TAB2 NZF (Fig. 8D). Considering that SHARPIN NZF but not HOIL-1L NZF can recognize K63-linked ubiquitin chains (Fig. 8A), these results indicate that WT SHARPIN is associated with K63-linked ubiquitin chains and that this association is abolished when its NZF domain is deleted (ΔNZF) or exchanged with HOIL-1L NZF.

SHARPIN T351F/L352V did not effectively suppress TNF-α-induced cell death relative to WT SHARPIN but did suppress cell death at levels comparable to SHARPIN ΔNZF (Fig. 8E and F), suggesting that ubiquitin recognition via the SHARPIN NZF but not the HOIL-1L NZF is essential for effective protection against TNF-α-induced cell death. These results collectively indicate that recognition of K63-linked ubiquitin chains via the SHARPIN NZF is critical for LUBAC recruitment to the activated TNFR complex to activate the canonical NF-κB pathway, as well as to inhibit programmed cell death.

DISCUSSION

The LUBAC ubiquitin ligase complex is composed of the HOIP catalytic subunit, the HOIL-1L accessory subunit, and the SHARPIN accessory subunit (8–10, 13–15). Although LUBAC is involved in canonical NF-κB activation as well as cell death regulation, loss of any of the three subunits yields distinct phenotypes (9, 13–16, 29, 30, 38, 39). In this study, we showed that loss of both HOIL-1L and SHARPIN in HOIL-1L$^{-/-}$ SHARPIN$^{cpdm/cpdm}$ mice produced an embryonic lethal phenotype at the same gestational stage (E10.5) as that observed for HOIP$^{-/-}$ mice due to augmented programmed cell death (Fig. 1A, B, E, and F). This was also the case for HOIP$^{\Delta linear/\Delta linear}$ mice, in which the ubiquitin ligase activity of LUBAC is lost (Fig. 1C to F). Since loss of both SHARPIN and HOIL-1L in MEFs overturned NF-κB activation and antagonized programmed cell death as observed in HOIP$^{\Delta linear/\Delta linear}$ MEFs (Fig. 5C, F, G, J, and K), a tiny amount of HOIP, which can be still detected in MEFs derived from HOIL-1L$^{-/-}$ SHARPIN$^{cpdm/cpdm}$ mice, is catalytically nonfunctional when both accessory subunits are absent (Fig. 5A). Our observations might be explained by a previous report showing that the N-terminal portion of HOIP autoinhibits its RING-IBR-RING domain and that either HOIL-1L or SHARPIN is required for the release of HOIP autoinhibition to restore ligase activity (40). Although necrostatin-1 could effectively protect HOIL-1L$^{+/-}$ SHARPIN$^{cpdm/cpdm}$ MEFs from TNF-α-mediated death, both necrostatin-1 and z-VAD were necessary for effective protection of HOIL-1L$^{-/-}$ SHARPIN$^{cpdm/cpdm}$ and HOIP$^{\Delta linear/\Delta linear}$ MEFs from death (Fig. 5I to K). Thus, the residual LUBAC ligase activity in HOIL-1L$^{+/-}$ SHARPIN$^{cpdm/cpdm}$ mice might be involved in the protection from embryonic lethality of mice by effecting cell evasion from unidentified RIP1-independent, caspase-dependent death, at least in part. Because both HOIL-1L$^{-/-}$ SHARPIN$^{cpdm/cpdm}$ and HOIP$^{\Delta linear/\Delta linear}$ mice are phenotypically similar to HOIP$^{-/-}$ mice (16), our present findings imply that the embryonic lethality of HOIP$^{-/-}$ mice is provoked by the loss of LUBAC linear ubiquitination activity. More importantly, our analyses clearly showed that the essential functional components of LUBAC required to generate linear polyubiquitin chains are HOIL-1L, SHARPIN, and HOIP. Structural analyses might reveal the precise stoichiometry of LUBAC, including how SHARPIN and HOIL-1L coordinately augment complex stability.

Our intercrossing analyses of HOIL-1L KO and cpdm mice clearly showed that SHARPIN is essential for protection against the onset of inflammatory diseases in cpdm mice, while introduction of two HOIL-1L KO alleles into mice failed to provoke any pathological lesions. However, HOIL-1L reduction did contribute to disease severity in mice lacking SHARPIN, although the subunit did not exert further qualitative histological changes in the affected organs or tissues (Fig. 3). Furthermore, no overt lesions were observed in HOIL-1L KO mice, at least at 12 weeks of age (Fig. 2A to C). Therefore, HOIL-1L seems to contribute mainly to the severity of inflammatory changes in mice by determining the expression level of LUBAC in concert with SHARPIN but does not provoke inflammatory disease by itself. Thus, SHARPIN deficiency causes cpdm symptoms from two aspects: attenuated protection against programmed cell death (caused specifically by loss of SHARPIN but not HOIL-1L) and LUBAC reduction due to destabilization of the complex (caused by loss of either SHARPIN or HOIL-1L).

We previously observed that an interferon-mediated increase in LUBAC composed of HOIL-1L and HOIP ameliorates, but cannot completely cure, cpdm symptoms (31). Given that HOIP levels were lower in interferon-treated cpdm keratinocytes than in WT keratinocytes, augmented activation of antiapoptotic NF-κB mediated by an increase in HOIL-1L/HOIP-containing LUBAC might not be able to completely override the augmented cell death

caused by loss of SHARPIN. Some humans lacking HOIL-1L, however, exhibit autoinflammation and immunodeficiency in addition to amylopectinosis in early childhood (30), whereas in other cases, mutations in the HOIL-1L gene cause various degrees of myopathies without immunological symptoms beginning in childhood or the juvenile years (39, 41). We have not observed any overt inflammatory diseases in HOIL-1L KO or HOIL-1L$^{-/-}$ SHARPIN$^{+/cpdm}$ mice, at least by 12 weeks of age (Fig. 2A to C), even though a recent report showed the presence of periodic acid-Schiff (PAS) stain-positive cytoplasmic inclusions in the myocardium of aged HOIL-1L KO mice (42). However, the observation that HOIL-1L contributes to the severity of inflammatory diseases provoked by SHARPIN loss in mice (Fig. 3) implies its involvement in inflammatory diseases in humans. These results suggest that HOIL-1L might function differently in humans and mice. Further analyses in mice and humans are required to clarify the precise roles of HOIL-1L in the LUBAC complex.

The identified major functions of LUBAC are canonical NF-κB activation and protection against programmed cell death. HOIL-1L and SHARPIN, the two regulatory subunits of LUBAC, are involved in the former (9, 13). However, SHARPIN, but not HOIL-1L, effectively protects cells against programmed death (Fig. 6E and F). Therefore, we turned our focus to dissection of the SHARPIN domains responsible for cell death protection (Fig. 6 and 7). To our surprise, the SHARPIN UBL and NZF domains, both of which are highly homologous to the HOIL-1L UBL and NZF domains, are contributors to this process (Fig. 6 and 7). Deletion of SHARPIN UBL exhibited a more profound effect than deletion of SHARPIN NZF, mainly by increasing the amount of LUBAC (Fig. 6B and C). Nevertheless, although HOIL-1L increased LUBAC to a far greater extent than SHARPIN when introduced into HOIL-1L$^{-/-}$ SHARPIN$^{cpdm/cpdm}$ MEFs, SHARPIN protected cells against TNF-α-mediated death much more effectively than HOIL-1L (Fig. 6D to G). Introduction of WT SHARPIN and its mutant (ΔN-term) containing the SHARPIN NZF domain likewise protected cpdm MEFs more effectively than introduction of SHARPIN mutants lacking the NZF domain (UBL, ΔNZF), although the effect mediated by NZF seemed less drastic than that mediated by UBL (Fig. 6B, H, and I).

The introduction of HOIL-1L or SHARPIN mutants with interchanged NZFs into HOIL-1L$^{-/-}$ SHARPIN$^{cpdm/cpdm}$ MEFs revealed that the SHARPIN NZF more effectively safeguarded against TNF-α-mediated cell death than the HOIL-1L NZF (Fig. 7). As the NZF domain is known as the ubiquitin-binding domain, we speculated that the functional differences between the SHARPIN and HOIL-1L NZFs might arise from differential affinities for ubiquitin chains with different linkages. In support of this hypothesis, the SHARPIN NZF, but not the HOIL-1L NZF, bound to K63-linked ubiquitin chains, while both NZFs bound to linear ubiquitin chains (Fig. 8A). We further demonstrated that recognition of K63-linked ubiquitin chains via the SHARPIN NZF, but not the HOIL-1L NZF, was indispensable for the effective recruitment of LUBAC to the activated TNFR complex, which mediates activation of canonical NF-κB (Fig. 8B to D), as well as protection against programmed cell death (Fig. 8E and F).

K63-linked ubiquitin chains generated by ubiquitin E3 ligases, including the cIAP ligases, are necessary for the recruitment of LUBAC to the activated receptor complex, since deletion of cIAPs inhibits recruitment of LUBAC to the activated TNF receptor complex (10). Also, we previously showed that the recruitment-promoting HOIP NZF1 domain recognizes K63-linked chains (11). Our present results suggest that the SHARPIN NZF functions in concert with the HOIP NZF1 to direct LUBAC to the TNFR complex. Because recognition of K63-linked chains by the SHARPIN NZF does not seem to be particularly robust based on a pulldown assay (Fig. 8A), the two domains might function in coordination to increase the affinity for K63-linked ubiquitin chains. Furthermore, the affinity of the HOIL-1L NZF for K63-linked chains is much weaker than that of the SHARPIN NZF (Fig. 8A). Accordingly, LUBAC composed of HOIL-1L and HOIP, which exists in cpdm cells, might be recruited to the TNFR complex less effectively than LUBAC composed of SHARPIN and HOIP, which is found in HOIL-1L KO cells upon stimulation with TNF-α. Therefore, the loss of SHARPIN likely may sensitize cells to programmed cell death to a greater extent than the loss of HOIL-1L due to impaired recruitment of LUBAC to the complex.

It has been suggested that ubiquitin ligase activity of LUBAC is a prerequisite for the retention of LUBAC to the activated receptor complex (10). LUBAC is, so far, believed to be the only E3 ligase that specifically generates M1-linked linear ubiquitin chains. Therefore, the NZF domain of HOIL-1L, which specifically recognizes M1-linked ubiquitin, might be important for LUBAC retention by recognizing linear ubiquitin chains attached to substrates, such as RIP1, in concert with the SHARPIN NZF, which can also bind to linear chains (15, 19).

As noted above, we showed that the SHARPIN NZF functions to recruit LUBAC to the activated receptor complex, possibly in concert with HOIP NZF1. Because LUBAC reportedly has a catalytic-independent role in NF-κB activation via antigen receptor signaling in lymphocytes (43), it might act as a scaffold protein complex as well as a ubiquitin ligase to specifically conjugate linear ubiquitin chains onto putative substrates, thereby regulating programmed cell death. Either way, as many as four types of NZF domains in the LUBAC ubiquitin ligase complex potentially contribute to the sophisticated regulation of LUBAC function by virtue of their diverse ubiquitin recognition modes. It will be extremely important to identify how this exquisite ubiquitin recognition system contributes to LUBAC-mediated actions in the context of the TNFR complex, including protection against programmed cell death.

ACKNOWLEDGMENTS

S.S. is supported by a Research Fellowship for Young Scientists from the Japan Society for the Promotion of Science.

We thank Keiko Okamoto-Furuta and Haruyasu Kohda (Division of Electron Microscopic Study, Center for Anatomical Studies, Graduate School of Medicine, Kyoto University) for skillful technical assistance in electron microscopy. Preparation of the paraffin-embedded sections was supported by the Anatomic Pathology Center of the Graduate School of Medicine of Kyoto University. We thank Toshio Kitamura (the Institute of Medical Science, University of Tokyo) for providing the pMXs-IP retroviral mammalian expression plasmid. We thank Yukiko Takeda, Katsuhiro Sasaki, and Erik Walinda for insightful discussions and Tomoko Nakagawa, Ai Himeno, and Sachiko Asano for assistance with animal care and genotyping of mice.

S.S., H.F., Y.S., K.F, and K.I. designed the research; S.S. and K.I. wrote the manuscript; S.S. and H.F. performed the experiments and prepared the figures; and T.T. performed the pathology analyses.

We declare no financial conflict of interests in association with this study.

FUNDING INFORMATION

This work, including the efforts of Kazuhiro Iwai, was funded by Ministry of Education, Culture, Sports, Science, and Technology (MEXT) (24112022, 25253019, and 26670514). This work, including the efforts of Satoshi Shimizu, was funded by Japan Society for the Promotion of Science (JSPS) (14J0189). This work, including the efforts of Kazuhiro Iwai, was funded by Takeda Science Foundation. This work, including the efforts of Kazuhiro Iwai, was funded by Naito Foundation. This work, including the efforts of Kazuhiro Iwai, was funded by Uehara Memorial Foundation.

REFERENCES

1. **Iwai K.** 2012. Diverse ubiquitin signaling in NF-κB activation. Trends Cell Biol **22:**355–364. http://dx.doi.org/10.1016/j.tcb.2012.04.001.
2. **Finley D.** 2009. Recognition and processing of ubiquitin-protein conjugates by the proteasome. Annu Rev Biochem **78:**477–513. http://dx.doi.org/10.1146/annurev.biochem.78.081507.101607.
3. **Deshaies RJ, Joazeiro CA.** 2009. RING domain E3 ubiquitin ligases. Annu Rev Biochem **78:**399–434. http://dx.doi.org/10.1146/annurev.biochem.78.101807.093809.
4. **Vucic D, Dixit VM, Wertz IE.** 2011. Ubiquitylation in apoptosis: a post-translational modification at the edge of life and death. Nat Rev Mol Cell Biol **12:**439–452. http://dx.doi.org/10.1038/nrm3143.
5. **Komander D, Rape M.** 2012. The ubiquitin code. Annu Rev Biochem **81:**203–229. http://dx.doi.org/10.1146/annurev-biochem-060310-170328.
6. **Dikic I, Wakatsuki S, Walters KJ.** 2009. Ubiquitin-binding domains—from structures to functions. Nat Rev Mol Cell Biol **10:**659–671. http://dx.doi.org/10.1038/nrm2767.
7. **Husnjak K, Dikic I.** 2012. Ubiquitin-binding proteins: decoders of ubiquitin-mediated cellular functions. Annu Rev Biochem **81:**291–322. http://dx.doi.org/10.1146/annurev-biochem-051810-094654.
8. **Kirisako T, Kamei K, Murata S, Kato M, Fukumoto H, Kanie M, Sano S, Tokunaga F, Tanaka K, Iwai K.** 2006. A ubiquitin ligase complex assembles linear polyubiquitin chains. EMBO J **25:**4877–4887. http://dx.doi.org/10.1038/sj.emboj.7601360.
9. **Tokunaga F, Sakata S, Saeki Y, Satomi Y, Kirisako T, Kamei K, Nakagawa T, Kato M, Murata S, Yamaoka S, Yamamoto M, Akira S, Takao T, Tanaka K, Iwai K.** 2009. Involvement of linear polyubiquitylation of NEMO in NF-κB activation. Nat Cell Biol **11:**123–132. http://dx.doi.org/10.1038/ncb1821.
10. **Haas TL, Emmerich CH, Gerlach B, Schmukle AC, Cordier SM, Rieser E, Feltham R, Vince J, Warnken U, Wenger T, Koschny R, Komander D, Silke J, Walczak H.** 2009. Recruitment of the linear ubiquitin chain assembly complex stabilizes the TNF-R1 signaling complex and is required for TNF-mediated gene induction. Mol Cell **36:**831–844. http://dx.doi.org/10.1016/j.molcel.2009.10.013.
11. **Fujita H, Rahighi S, Akita M, Kato R, Sasaki Y, Wakatsuki S, Iwai K.** 2014. Mechanism underlying IκB kinase activation mediated by the linear ubiquitin chain assembly complex. Mol Cell Biol **34:**1322–1335. http://dx.doi.org/10.1128/MCB.01538-13.
12. **Rahighi S, Ikeda F, Kawasaki M, Akutsu M, Suzuki N, Kato R, Kensche T, Uejima T, Bloor S, Komander D, Randow F, Wakatsuki S, Dikic I.** 2009. Specific recognition of linear ubiquitin chains by NEMO is important for NF-κB activation. Cell **136:**1098–1109. http://dx.doi.org/10.1016/j.cell.2009.03.007.
13. **Tokunaga F, Nakagawa T, Nakahara M, Saeki Y, Taniguchi M, Sakata S, Tanaka K, Nakano H, Iwai K.** 2011. SHARPIN is a component of the NF-κB-activating linear ubiquitin chain assembly complex. Nature **471:**633–636. http://dx.doi.org/10.1038/nature09815.
14. **Ikeda F, Deribe YL, Skanland SS, Stieglitz B, Grabbe C, Franz-Wachtel M, van Wijk SJ, Goswami P, Nagy V, Terzic J, Tokunaga F, Androulidaki A, Nakagawa T, Pasparakis M, Iwai K, Sundberg JP, Schaefer L, Rittinger K, Macek B, Dikic I.** 2011. SHARPIN forms a linear ubiquitin ligase complex regulating NF-κB activity and apoptosis. Nature **471:**637–641. http://dx.doi.org/10.1038/nature09814.
15. **Gerlach B, Cordier SM, Schmukle AC, Emmerich CH, Rieser E, Haas TL, Webb AI, Rickard JA, Anderton H, Wong WW, Nachbur U, Gangoda L, Warnken U, Purcell AW, Silke J, Walczak H.** 2011. Linear ubiquitination prevents inflammation and regulates immune signalling. Nature **471:**591–596. http://dx.doi.org/10.1038/nature09816.
16. **Peltzer N, Rieser E, Taraborrelli L, Draber P, Darding M, Pernaute B, Shimizu Y, Sarr A, Draberova H, Montinaro A, Martinez-Barbera JP, Silke J, Rodriguez TA, Walczak H.** 2014. HOIP deficiency causes embryonic lethality by aberrant TNFR1-mediated endothelial cell death. Cell Rep **9:**153–165. http://dx.doi.org/10.1016/j.celrep.2014.08.066.
17. **Rickard JA, Anderton H, Etemadi N, Nachbur U, Darding M, Peltzer N, Lalaoui N, Lawlor KE, Vanyai H, Hall C, Bankovacki A, Gangoda L, Wong WW, Corbin J, Huang C, Mocarski ES, Murphy JM, Alexander WS, Voss AK, Vaux DL, Kaiser WJ, Walczak H, Silke J.** 2 December 2014. TNFR1-dependent cell death drives inflammation in Sharpin-deficient mice. eLife **3:**e03464. http://dx.doi.org/10.7554/eLife.03464.
18. **Kumari S, Redouane Y, Lopez-Mosqueda J, Shiraishi R, Romanowska M, Lutzmayer S, Kuiper J, Martinez C, Dikic I, Pasparakis M, Ikeda F.** 2 December 2014. Sharpin prevents skin inflammation by inhibiting TNFR1-induced keratinocyte apoptosis. eLife **3:**e03422. http://dx.doi.org/10.7554/eLife.03422.
19. **Sato Y, Fujita H, Yoshikawa A, Yamashita M, Yamagata A, Kaiser SE, Iwai K, Fukai S.** 2011. Specific recognition of linear ubiquitin chains by the Npl4 zinc finger (NZF) domain of the HOIL-1L subunit of the linear ubiquitin chain assembly complex. Proc Natl Acad Sci U S A **108:**20520–20525. http://dx.doi.org/10.1073/pnas.1109088108.
20. **Lim S, Sala C, Yoon J, Park S, Kuroda S, Sheng M, Kim E.** 2001. Sharpin, a novel postsynaptic density protein that directly interacts with the Shank family of proteins. Mol Cell Neurosci **17:**385–397. http://dx.doi.org/10.1006/mcne.2000.0940.
21. **Alam SL, Sun J, Payne M, Welch BD, Blake BK, Davis DR, Meyer HH, Emr SD, Sundquist WI.** 2004. Ubiquitin interactions of NZF zinc fingers. EMBO J **23:**1411–1421. http://dx.doi.org/10.1038/sj.emboj.7600114.
22. **HogenEsch H, Gijbels MJ, Offerman E, van Hooft J, van Bekkum DW, Zurcher C.** 1993. A spontaneous mutation characterized by chronic proliferative dermatitis in C57BL mice. Am J Pathol **143:**972–982.
23. **Gijbels MJ ZC, Kraal G, Elliott GR, HogenEsch H, Schijff G, Savelkoul HF, Bruijnzeel PL.** 1996. Pathogenesis of skin lesions in mice with chronic proliferative dermatitis (cpdm/cpdm). Am J Pathol **148:**941–950.
24. **Iwai K.** 2011. Linear polyubiquitin chains: a new modifier involved in NFκB activation and chronic inflammation, including dermatitis. Cell Cycle **10:**3095–3104. http://dx.doi.org/10.4161/cc.10.18.17437.
25. **HogenEsch H, Janke S, Boggess D, Sundberg JP.** 1999. Absence of Peyer's patches and abnormal lymphoid architecture in chronic proliferative dermatitis (cpdm/cpdm) mice. J Immunol **162:**3890–3896.
26. **HogenEsch H, Torregrosa SE, Boggess D, Sundberg BA, Carroll J, Sundberg JP.** 2001. Increased expression of type 2 cytokines in chronic proliferative dermatitis (cpdm) mutant mice and resolution of inflammation following treatment with IL-12. Eur J Immunol **31:**734–742. http://dx.doi.org/10.1002/1521-4141(200103)31:3<734::AID-IMMU734>3.0.CO;2-9.
27. **Seymour RE, Hasham MG, Cox GA, Shultz LD, Hogenesch H, Roopenian DC, Sundberg JP.** 2007. Spontaneous mutations in the mouse Sharpin gene result in multiorgan inflammation, immune system dysregulation and dermatitis. Genes Immun **8:**416–421. http://dx.doi.org/10.1038/sj.gene.6364403.
28. **Berger SB, Kasparcova V, Hoffman S, Swift B, Dare L, Schaeffer M, Capriotti C, Cook M, Finger J, Hughes-Earle A, Harris PA, Kaiser WJ, Mocarski ES, Bertin J, Gough PJ.** 2014. Cutting Edge: RIP1 kinase activity is dispensable for normal development but is a key regulator of inflammation in SHARPIN-deficient mice. J Immunol **192:**5476–5480. http://dx.doi.org/10.4049/jimmunol.1400499.
29. **Sasaki Y, Sano S, Nakahara M, Murata S, Kometani K, Aiba Y, Sakamoto S, Watanabe Y, Tanaka K, Kurosaki T, Iwai K.** 2013. Defective immune responses in mice lacking LUBAC-mediated linear ubiquitination in B cells. EMBO J **32:**2463–2476. http://dx.doi.org/10.1038/emboj.2013.184.
30. **Boisson B, Laplantine E, Prando C, Giliani S, Israelsson E, Xu Z, Abhyankar A, Israel L, Trevejo-Nunez G, Bogunovic D, Cepika AM, MacDuff D, Chrabieh M, Hubeau M, Bajolle F, Debre M, Mazzolari E, Vairo D, Agou F, Virgin HW, Bossuyt X, Rambaud C, Facchetti F, Bonnet D, Quartier P, Fournet JC, Pascual V, Chaussabel D, Notarangelo LD, Puel A, Israel A, Casanova JL, Picard C.** 2012. Immunodeficiency, autoinflammation and amylopectinosis in humans with inherited HOIL-1 and LUBAC deficiency. Nat Immunol **13:**1178–1186. http://dx.doi.org/10.1038/ni.2457.
31. **Tamiya H, Terao M, Takiuchi T, Nakahara M, Sasaki Y, Katayama I, Yoshikawa H, Iwai K.** 2014. IFN-γ or IFN-α ameliorates chronic

proliferative dermatitis by inducing expression of linear ubiquitin chain assembly complex. J Immunol **192:**3793–3804. http://dx.doi.org/10.4049/jimmunol.1302308.

32. **Sakurai H, Chiba H, Miyoshi H, Sugita T, Toriumi W.** 1999. IκB kinases phosphorylate NF-κB p65 subunit on serine 536 in the transactivation domain. J Biol Chem **274:**30353–30356. http://dx.doi.org/10.1074/jbc.274.43.30353.
33. **Vandenabeele P, Galluzzi L, Vanden Berghe T, Kroemer G.** 2010. Molecular mechanisms of necroptosis: an ordered cellular explosion. Nat Rev Mol Cell Biol **11:**700–714. http://dx.doi.org/10.1038/nrm2970.
34. **Festjens N, Vanden Berghe T, Cornelis S, Vandenabeele P.** 2007. RIP1, a kinase on the crossroads of a cell's decision to live or die. Cell Death Differ **14:**400–410. http://dx.doi.org/10.1038/sj.cdd.4402085.
35. **Kaczmarek A, Vandenabeele P, Krysko DV.** 2013. Necroptosis: the release of damage-associated molecular patterns and its physiological relevance. Immunity **38:**209–223. http://dx.doi.org/10.1016/j.immuni.2013.02.003.
36. **Dynek JN, Goncharov T, Dueber EC, Fedorova AV, Izrael-Tomasevic A, Phu L, Helgason E, Fairbrother WJ, Deshayes K, Kirkpatrick DS, Vucic D.** 2010. c-IAP1 and UbcH5 promote K11-linked polyubiquitination of RIP1 in TNF signalling. EMBO J **29:**4198–4209. http://dx.doi.org/10.1038/emboj.2010.300.
37. **Sato Y, Yoshikawa A, Yamashita M, Yamagata A, Fukai S.** 2009. Structural basis for specific recognition of Lys 63-linked polyubiquitin chains by NZF domains of TAB2 and TAB3. EMBO J **28:**3903–3909. http://dx.doi.org/10.1038/emboj.2009.345.
38. **Boisson B, Laplantine E, Dobbs K, Cobat A, Tarantino N, Hazen M, Lidov HG, Hopkins G, Du L, Belkadi A, Chrabieh M, Itan Y, Picard C, Fournet JC, Eibel H, Tsitsikov E, Pai SY, Abel L, Al-Herz W, Casanova JL, Israel A, Notarangelo LD.** 2015. Human HOIP and LUBAC deficiency underlies autoinflammation, immunodeficiency, amylopectinosis, and lymphangiectasia. J Exp Med **212:**939–951. http://dx.doi.org/10.1084/jem.20141130.
39. **Wang K, Kim C, Bradfield J, Guo Y, Toskala E, Otieno FG, Hou C, Thomas K, Cardinale C, Lyon GJ, Golhar R, Hakonarson H.** 2013. Whole-genome DNA/RNA sequencing identifies truncating mutations in RBCK1 in a novel Mendelian disease with neuromuscular and cardiac involvement. Genome Med **5:**67. http://dx.doi.org/10.1186/gm471.
40. **Stieglitz B, Morris-Davies AC, Koliopoulos MG, Christodoulou E, Rittinger K.** 2012. LUBAC synthesizes linear ubiquitin chains via a thioester intermediate. EMBO Rep **13:**840–846. http://dx.doi.org/10.1038/embor.2012.105.
41. **Nilsson J, Schoser B, Laforet P, Kalev O, Lindberg C, Romero NB, Davila Lopez M, Akman HO, Wahbi K, Iglseder S, Eggers C, Engel AG, Dimauro S, Oldfors A.** 2013. Polyglucosan body myopathy caused by defective ubiquitin ligase RBCK1. Ann Neurol **74:**914–919. http://dx.doi.org/10.1002/ana.23963.
42. **MacDuff DA, Reese TA, Kimmey JM, Weiss LA, Song C, Zhang X, Kambal A, Duan E, Carrero JA, Boisson B, Laplantine E, Israel A, Picard C, Colonna M, Edelson BT, Sibley LD, Stallings CL, Casanova JL, Iwai K, Virgin HW.** 20 January 2015. Phenotypic complementation of genetic immunodeficiency by chronic herpesvirus infection. eLife **4:**e04494. http://dx.doi.org/10.7554/eLife.04494.
43. **Dubois SM, Alexia C, Wu Y, Leclair HM, Leveau C, Schol E, Fest T, Tarte K, Chen ZJ, Gavard J, Bidere N.** 2014. A catalytic-independent role for the LUBAC in NF-κB activation upon antigen receptor engagement and in lymphoma cells. Blood **123:**2199–2203. http://dx.doi.org/10.1182/blood-2013-05-504019.